

Hadron spectrum with Wilson fermions

Tanmoy Bhattacharya and Rajan Gupta

T-8, MS-B285, Los Alamos National Laboratory, Los Alamos, New Mexico 87545

Gregory Kilcup

Physics Department, The Ohio State University, Columbus, Ohio 43210

Stephen Sharpe

Physics Department, University of Washington, Seattle, Washington 98195

(Received 22 December 1995)

We present results of a high statistics study of the quenched spectrum using Wilson fermions at $\beta=6.0$ on $32^3 \times 64$ lattices. We calculate the masses of mesons and baryons composed of both degenerate and nondegenerate quarks. Using nondegenerate quark combinations allows us to study baryon mass splittings in detail. We find significant deviations from the lowest order chiral expansion, deviations that are consistent with the expectations of quenched chiral perturbation theory. We find that there is a $\sim 20\%$ systematic error in the extracted value of m_s , depending on the meson mass ratio used to set its value. Using the largest estimate of m_s we find that the extrapolated octet mass splittings are in agreement with the experimental values, as is $M_\Delta - M_N$, while the decuplet splittings are 30% smaller than experiment. Combining our results with data from the GF11 collaboration we find considerable ambiguity in the extrapolation to the continuum limit. Our preferred values are $M_N/M_\rho = 1.38(7)$ and $M_\Delta/M_\rho = 1.73(10)$, suggesting that the quenched approximation is good to only $\sim 10-15\%$. We also analyze the $O(ma)$ discretization errors in heavy quark masses. [S0556-2821(96)02311-9]

PACS number(s): 12.38.Gc, 14.20.-c, 14.40.-n

I. INTRODUCTION

Precise measurements of the hadron spectrum using lattice QCD are crucial both to validate QCD as the correct theory of strong interactions and to establish the reliability of numerical simulations for extracting weak matrix elements. Current lattice calculations suffer from a variety of systematic errors, most notably those due to quenching, discretization, and the need to extrapolate to light quark masses. In this work we present a detailed study of these systematics for the hadron spectrum.

Such a study requires small statistical errors. We have reduced these by using a moderately large ensemble, 170 lattices, and working on a large lattice, $32^3 \times 64$ at $\beta=6.0$, in the quenched approximation. We use unimproved Wilson fermions. Preliminary results from a subset of 100 lattices were presented at the Lattice '94 meeting [1]. Our lattices are large enough that we expect finite size effects to be small. The major technical features of our work are (a) using two kinds of sources that yield correlators that converge to their asymptotic values from opposite directions, so as to improve the reliability of the masses extracted; (b) calculating hadron masses using nondegenerate light quarks, which allows us to study the quark-mass dependence in detail; and (c) using ratios of correlators to obtain accurate estimates of mass differences. We find that terms of higher order than linear in the quark mass are very significant and that their inclusion is essential for the extrapolation to the physical light quark masses, particularly for mass splittings among spin-1/2 baryons. Higher order terms are also important for vector mesons and spin-3/2 baryons.

The outline of the paper is as follows. In the following

section we explain how we generate lattices and calculate quark propagators. After a brief discussion of the fitting and a summary of the expected chiral behavior of hadron masses in the quenched approximation, we present our results for mesons and baryon masses. We then extrapolate mass ratios to the continuum limit by combining our results with those of the GF11 collaboration [2]. There turns out to be considerable ambiguity in this extrapolation. Our preferred values for the extrapolated ratios are $M_N/M_\rho = 1.38(7)$ and $M_\Delta/M_\rho = 1.73(10)$. This suggests that the quenched approximation is good to $\sim 10-15\%$, less accurate than suggested in Ref. [2]. We close with some conclusions and suggestions for further work.

We use the following conventions throughout the paper. Hadron masses are denoted by an uppercase M , while for quark masses we use a lowercase m . All masses are in lattice units unless explicitly expressed in MeV (or GeV).

II. DETAILS OF SIMULATIONS

Gauge configurations are generated using a combination of overrelaxed (OR), pseudo-heat-bath (PHB), and Metropolis algorithms. Typically, five (OR) sweeps are followed by a PHB update, with the latter consisting of three hits, one in each of the SU(2) subgroups. In some cases the PHB update is replaced by a 20-hit Metropolis sweep. Two independent streams were generated, each starting from a lattice consisting of two independently thermalized 32^4 lattices joined together. A further $2000 \times (5\text{OR} + 1\text{PHB})$ thermalization sweeps were then performed. Thereafter we analyze lattices separated by $400 \times (5\text{OR} + 1\text{PHB})$ sweeps.

We calculate quark propagators using the simple Wilson

action, with periodic boundary conditions in all four directions. We use two kinds of extended sources, Wuppertal and Wall, at each of the five values of quark mass given by $\kappa=0.135$ (C), 0.153 (S), 0.155 (U_1), 0.1558 (U_2), and 0.1563 (U_3). These quarks correspond to pseudoscalar mesons of mass 2835, 983, 690, 545, and 431 MeV, respectively, using $1/a=2.33$ GeV for the lattice scale. We use the three light quarks to extrapolate the data to the physical isospin symmetric light quark mass $\bar{m}=(m_u+m_d)/2$, while the C and S κ values are selected to be close to the physical charm and strange quark masses. The physical value of the strange quark, in fact, lies between S and U_1 , and we use these two points to interpolate to it. In most cases we find that the extrapolation to \bar{m} can be done using the six combinations of light quarks, U_1U_1 , U_1U_2 , U_1U_3 , U_2U_2 , U_2U_3 , and U_3U_3 . For brevity we use $\{U_iU_j\}$ to refer to this set of masses.

We analyze three types of hadron correlators distinguished by the sources and sinks used to generate quark propagators. These are wall source and point sink (WL), Wuppertal source and point sink (SL), and Wuppertal source and sink (SS). The notation and details of the implementation of the Wuppertal source are as in our previous work [3]. The smearing parameter is set to $\kappa_{KG}=0.181$, corresponding to a smearing size of $\Omega^2\approx 3$. (In [3] this was mistakenly written as $\Omega\approx 3$.) The generation of the Wuppertal sources is a negligible overhead on the inversion.

The Dirac equation is solved using the overrelaxed preconditioned (fourth order polynomial) minimal residue (MR4) algorithm described in Ref. [4]. The convergence rate is quite insensitive to the overrelaxation parameter ω as long as it is in the range 1.2–1.35; we use $\omega=1.3$. We set the convergence criteria (for all values of κ) to $|r^2|/|\chi^2|<10^{-14}$, where r is the remainder and χ is the solution. This tolerance is as small as we can demand, as we use IEEE single precision arithmetic. To ensure convergence we run the MR4 inverter up to three times, refreshing the starting remainder each time, and then switch to a conjugate gradient, and force it to run at least one cycle. To date, we have observed no failures of MR4. We note that the simple MR algorithms are much less sensitive to our use of 32-bit arithmetic than the CG-based algorithms, whose convergence rate depends on maintaining orthogonality of a sequence of vectors. Indeed, we have found that MR4 is one of the most efficient and stable of the algorithms (MR, MR2, MR4, CG, BiCG5 [5], and BiCGStab [6]), we have implemented on the CM5.

A technical detail of our MR4 algorithm that makes it suitable for 32-bit precision is as follows. The n th iterate of the solution χ (and similarly the remainder r) is given by $\vec{\chi}_n = \vec{\chi}_{n-1} + \omega\alpha_n\vec{r}_{n-1}$. The global sums needed in the calculation of α_n are done in double precision. Any residual errors $\delta\alpha_n$ can be absorbed into ω and do not adversely affect the convergence rate as long as $\omega_n = \omega(1 + \delta\alpha_n)$ stays within the optimal range. Our tests also show that the calculation of α_n can be done in single precision and that the convergence rate is not affected provided the remainder is refreshed somewhat more often depending on the quark mass.

The only place that round-off errors due to use of 32-bit precision could affect the results is in the evaluation of the final convergence. For this purpose we make two checks. First, we monitor the final value of $|r^2|$ and $|r^2|/|\chi^2|$ on each

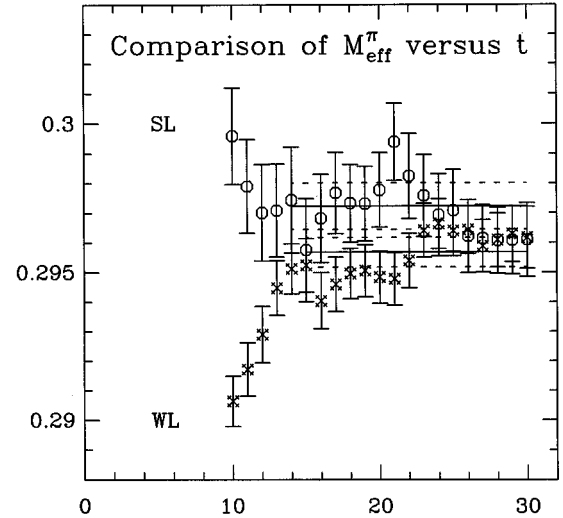


FIG. 1. Comparison of $M_{\text{eff}}(t)$ for U_1U_1 pion correlators with SL and WL sources.

time slice in addition to the global value which could be biased by time slices closest to the source. We find that the values at the time slice farthest from the source are $|r^2|/|\chi^2|\approx 10^{-6}$ for the C quark and $\leq 10^{-13}$ for other quarks. This means that, even for the heaviest quark, the effect of incomplete convergence is smaller than the statistical errors. Second, we double the number of inversion sweeps on randomly selected lattices. We find that the relative change in the value of hadronic two-point correlation functions is $\leq 10^{-5}$, which is negligible.

III. FITTING

To illustrate some of the issues involved in fitting, we show, in Figs. 1–3, representative results for the effective mass. We define this as $M_{\text{eff}}(t) = \ln[C(t-1)/C(t)]$, plus corrections due to periodicity in the time direction. The source lies at $t=0$ in all plots. It is a general feature that the WL effective masses approach their asymptotic value from

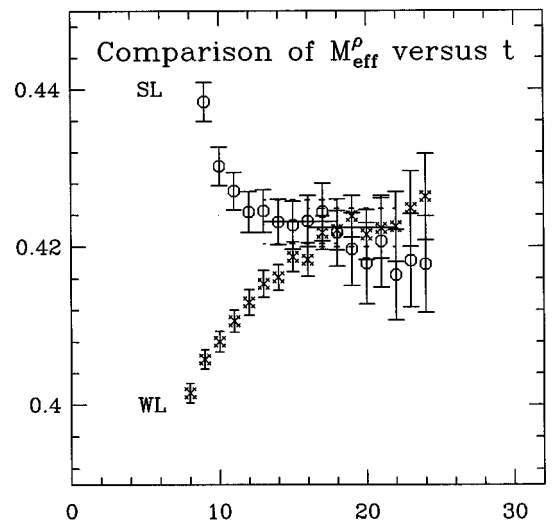


FIG. 2. Comparison of $M_{\text{eff}}(t)$ for U_1U_1 ρ correlators with SL and WL sources.

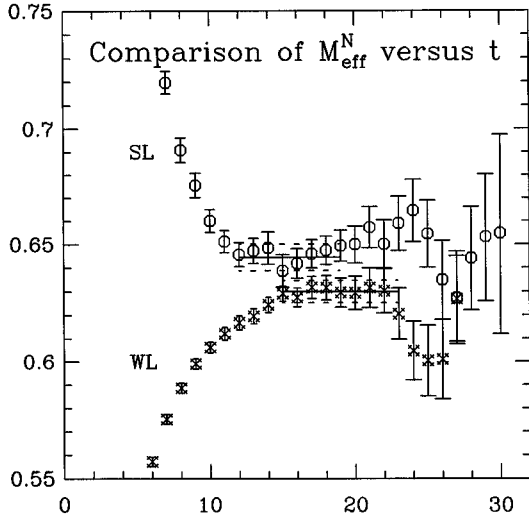


FIG. 3. Comparison of $M_{\text{eff}}(t)$ for $U_1U_1U_1$ nucleon correlators with *SL* and *WL* sources.

below, while those for *SL* and *SS* correlators approach from above. We consider in turn the problems we face and the solutions we have adopted.

(1) A major problem is that, at the 2σ level, the convergence to the asymptotic value of M_{eff} is extremely slow. The *SL* and *WL* effective masses do come together eventually for pion and ρ correlators, but for the nucleon the signal disappears into noise before convergence has occurred. Masses extracted from *WL* correlators are systematically lower than those from *SL* or *SS* correlators. For the pion and ρ channels, this difference is $\sim 1\sigma$, while for the nucleons it is $\sim (2-3)\sigma$.

We think that this behavior is mainly due to limited statistics—a recent study by the JLQCD Collaboration [7] indicates that fluctuations at the 2σ level are the rule rather than the exception. What we have done in practice is to average the masses with weightings $(2\text{WL} + \text{SL} + \text{SS})/4$. The equal weighting of wall and Wuppertal sources ensures that the resulting mass lies between the two sets of data on the effective mass plot. Errors are obtained using single-elimination jackknife, performing a complete analysis (including forming the average masses) on each jackknife sample.

(2) The previous problem is exacerbated by the fact that we have been unable to do stable fitting using the full correlation matrix. When we do so, some fits lead to clearly unreasonable values for masses, presumably because small errors in the correlation matrix are magnified when this matrix is inverted to calculate χ^2 . This problem is well known, and various remedies have been proposed [8]. For example, one can project against the eigenvectors of the correlation matrix having small eigenvalues and then invert. Alternatively, one can reduce the range of times to which one fits. We have tried both schemes, but find that the resulting mass estimates are indistinguishable from those obtained fitting just with the diagonal elements of the correlation matrix (“uncorrelated fits”). Given that the schemes involve further subjective selections (e.g., how many eigenvectors to discard), we choose to use uncorrelated fits for our standard results. We do use the “correlated fits,” however, to check that our fits are rea-

sonable. Given that this is so, our jackknife errors should be reliable.

(3) In a similar spirit, we have chosen to use single mass fits for our final answers. We have also made fits with two masses, but find that these fits require considerable tuning by hand, because our minimization routines tend to give the same result for the two masses for a few of the jackknife samples. When we remove this problem, the resulting estimate for the lightest mass is consistent with that from the single mass fit, while the errors are 50% larger. Given the large number of correlators that we fit, it is impractical to do the tuning for each channel.

(4) Finally, we must choose a fit range. We choose the minimum time by inspecting the effective mass plots and deciding where the “plateau” region begins. The maximum time is then taken to be that at which the diagonal errors have roughly doubled compared to the beginning of the plateau or that at which the signal shows a clear break. For the pion correlator, where the errors do not grow with time, this means that we use all points beyond the minimum time.

Our overriding criterion is to include as many time slices as possible in the fits. We have not succeeded in developing a robust automated procedure that meets this objective when using two mass fits or incorporating the full covariance matrix. Since we analyze ~ 4000 channels, it is not practical to tune the fitting of each by hand. Thus, for consistency, we use, for all channels, single mass fits, keeping only the diagonal elements of the correlation matrix. We feel confident in both our central values and our error estimates, however, since in the many channels that we have fitted by hand, the results do not change significantly when we use the full correlation matrix and two mass fits.

IV. QUENCHING ERRORS

In the last few years it has been argued that, in the quenched approximation, the η' is a pseudo Goldstone boson and that η' loops give rise to chiral logarithms which make the quenched approximation singular in the chiral limit [9,10]. The same methods (“quenched chiral perturbation theory”) have been used to estimate the errors due to quenching. It is important to test the predictions of this theory against numerical results. There is some supporting evidence—see Refs. [11] and [12] for recent reviews—but more work is needed.

We collect here the results of quenched chiral perturbation theory relevant for this work. The expansion for the mass of a “pion” composed of quarks of mass m_1 and m_2 is

$$M_\pi^2 = c_\pi(m_1 + m_2)\{1 - \delta \ln[(m_1 + m_2)]\} + e_\pi m_q^2 + \dots, \quad (4.1)$$

with c_π , e_π , and δ constants and the ellipsis representing higher order terms in the chiral expansion. The m_q^2 term is shorthand both for analytic terms, i.e., those proportional to $(m_1 + m_2)^2$, m_1^2 , and m_2^2 , and for nonanalytic chiral logarithms of general form $m_q^2 \ln(m_q)$. Such terms are present both in quenched and in full QCD, although the constants multiplying them will be different in the two theories. In contrast, the δ term is an artifact of quenching—it arises from η' loops and is divergent in the chiral limit. Evidence for this divergence has been found with staggered fermions

TABLE I. Meson masses from WL correlators at $\vec{p}=0$. Errors shown are in the last two decimal places.

	π	A_4/A_4	A_4/π	π/A_4	ρ	a_0	a_1
CC	1.217(01)	1.217(00)	1.217(01)	1.217(01)	1.229(01)	1.432(06)	1.439(05)
CS	0.853(01)	0.854(01)	0.853(01)	0.854(01)	0.878(01)		1.104(04)
CU_1	0.813(01)	0.814(01)	0.813(01)	0.814(01)	0.841(01)		1.081(07)
CU_2	0.797(01)	0.798(01)	0.798(01)	0.798(01)	0.826(01)		1.080(10)
CU_3	0.787(01)	0.789(02)	0.789(02)	0.789(02)	0.816(02)		1.087(13)
SS	0.421(00)	0.421(01)	0.422(01)	0.421(01)	0.504(01)	0.743(15)	0.753(05)
SU_1	0.362(00)	0.363(01)	0.363(01)	0.362(01)	0.463(01)	0.720(18)	0.721(07)
SU_2	0.338(01)	0.338(01)	0.338(01)	0.337(01)	0.447(02)	0.743(31)	0.712(09)
SU_3	0.322(01)	0.322(01)	0.323(01)	0.321(01)	0.438(02)		0.714(12)
U_1U_1	0.296(01)	0.296(01)	0.296(01)	0.295(01)	0.422(02)	0.724(53)	0.685(09)
U_1U_2	0.266(01)	0.266(01)	0.267(01)	0.265(01)	0.404(03)		0.674(12)
U_1U_3	0.246(01)	0.247(01)	0.247(01)	0.245(01)	0.393(03)		0.672(15)
U_2U_2	0.233(01)	0.233(01)	0.234(01)	0.232(01)	0.386(03)		0.660(14)
U_2U_3	0.210(01)	0.210(01)	0.211(01)	0.209(01)	0.371(03)		0.656(18)
U_3U_3	0.184(01)	0.184(01)	0.186(01)	0.183(01)	0.359(04)		0.646(22)

[13], but the effect is small and becomes noticeable only at quark masses smaller than those we use. Thus when fitting the pion masses we ignore the δ term.

The predicted form for baryon masses is, schematically [14],

$$M_N = a_N + \delta[b_N m_q^{1/2} + b'_N m_q \ln(m_q)] + c_N m_q + d_N m_q^{3/2} + e_N m_q^2 + \dots, \quad (4.2)$$

where δ is the same constant as in Eq. (4.1), while $a_N - e_N$ are additional constants. The expansion has the same form in full QCD, except that the δ term, which again comes from η' loops, is absent. As for the pion, we ignore the δ term in almost all fits. It is small (because δ is small) and, furthermore, is numerically indistinguishable from the higher order terms within our range of light quark masses. What we can test in some detail, however, is the expected form of the m_q , $m_q^{3/2}$, and m_q^2 terms. Here we benefit greatly from our use of nondegenerate quarks.

Similar comments apply to the vector meson masses. Although these have not been discussed in the quenched chiral perturbation theory literature, it is straightforward to extend the work done in QCD [15] and arrive at the prediction

$$M_\rho = a_\rho + \delta b_\rho m_q^{1/2} + c_\rho(m_1 + m_2) + d_\rho m_q^{3/2} + e_\rho m_q^2 + \dots. \quad (4.3)$$

Unlike for baryons, the detailed expressions for b_ρ , c_ρ , and d_ρ in terms of constants in the quenched chiral Lagrangian are not known. Nevertheless, we expect that the δ term will be small and again ignore it in our fitting.

V. MESON MASSES

We give our results for meson masses in Tables I–IV. We quote separately the results for the three source-sink combinations and the average $(2WL+SL+SS)/4$. There are four columns for the pion in each table because we use Lorentz structures $\gamma_5=P$ and $\gamma_4\gamma_5=A_4$ for both source and sink.

TABLE II. Meson masses from SL correlators at $\vec{p}=0$.

	π	A_4/A_4	A_4/π	π/A_4	ρ	a_0	a_1
CC	1.217(01)	1.217(01)	1.217(01)	1.217(01)	1.230(01)	1.421(11)	1.448(09)
CS	0.854(01)	0.854(01)	0.855(01)	0.854(01)	0.881(01)	1.079(17)	1.126(12)
CU_1	0.815(01)	0.815(01)	0.815(01)	0.814(01)	0.844(02)	1.047(22)	1.097(15)
CU_2	0.800(02)	0.800(02)	0.800(02)	0.800(02)	0.829(02)	1.040(28)	1.089(18)
CU_3	0.791(02)	0.792(03)	0.791(02)	0.792(02)	0.821(03)	1.048(38)	1.090(23)
SS	0.423(01)	0.422(01)	0.423(01)	0.422(01)	0.506(02)	0.716(16)	0.777(13)
SU_1	0.364(01)	0.363(01)	0.364(01)	0.364(01)	0.464(03)	0.684(24)	0.741(16)
SU_2	0.340(01)	0.339(01)	0.340(01)	0.340(01)	0.450(03)	0.697(29)	0.731(19)
SU_3	0.324(01)	0.323(02)	0.324(01)	0.324(01)	0.440(03)	0.733(48)	0.729(22)
U_1U_1	0.297(01)	0.296(01)	0.297(01)	0.297(01)	0.423(03)	0.677(37)	0.705(20)
U_1U_2	0.268(01)	0.267(02)	0.268(01)	0.268(01)	0.406(04)	0.704(42)	0.695(25)
U_1U_3	0.248(01)	0.247(02)	0.248(02)	0.248(01)	0.396(05)	0.736(39)	0.695(29)
U_2U_2	0.235(01)	0.233(02)	0.235(02)	0.235(01)	0.389(05)		0.687(30)
U_2U_3	0.212(01)	0.210(02)	0.212(02)	0.212(02)	0.377(06)		0.688(36)
U_3U_3	0.186(01)	0.184(02)	0.186(02)	0.185(02)	0.363(08)		0.691(45)

TABLE III. Meson masses from SS correlators at $\vec{p}=0$.

	π	A_4/A_4	A_4/π	π/A_4	ρ	a_0	a_1
CC	1.218(01)	1.218(01)	1.218(01)	1.217(01)	1.230(01)	1.421(12)	1.438(11)
CS	0.854(01)	0.855(01)	0.855(01)	0.854(01)	0.880(01)	1.071(21)	1.118(15)
CU_1	0.814(01)	0.815(02)	0.815(01)	0.815(02)	0.843(02)	1.043(29)	1.084(19)
CU_2	0.799(02)	0.800(02)	0.800(02)	0.800(02)	0.829(02)	1.040(38)	1.074(23)
CU_3	0.791(02)	0.792(03)	0.791(03)	0.792(03)	0.820(03)	1.045(42)	1.072(28)
SS	0.422(01)	0.422(01)	0.422(01)	0.422(01)	0.507(02)	0.707(18)	0.770(14)
SU_1	0.364(01)	0.364(01)	0.364(01)	0.364(01)	0.465(02)	0.677(27)	0.738(13)
SU_2	0.340(01)	0.339(01)	0.340(01)	0.339(01)	0.449(03)	0.691(31)	0.725(19)
SU_3	0.324(01)	0.324(02)	0.324(01)	0.324(01)	0.440(03)	0.724(29)	0.726(16)
U_1U_1	0.297(01)	0.296(01)	0.297(01)	0.297(01)	0.422(03)	0.672(39)	0.702(15)
U_1U_2	0.268(01)	0.267(01)	0.268(01)	0.267(01)	0.405(04)	0.692(30)	0.691(17)
U_1U_3	0.248(01)	0.247(02)	0.248(01)	0.248(02)	0.395(05)	0.726(32)	0.687(20)
U_2U_2	0.235(01)	0.233(02)	0.235(01)	0.234(01)	0.387(05)		0.679(20)
U_2U_3	0.212(01)	0.210(02)	0.212(02)	0.211(02)	0.375(07)		0.675(24)
U_3U_3	0.186(01)	0.184(02)	0.186(02)	0.184(02)	0.361(08)		0.671(28)

Thus PP has a pseudoscalar interpolating field at both source and sink, while PA_4 has an axial interpolating field at the sink. The four possibilities yield consistent results for masses, and we use the average of the four (inside our jack-knife loop) to give our best estimate of M_π .

States at $\vec{p}=0$ created by $\bar{\psi}\psi$ are labeled a_0 and those by $\bar{\psi}\gamma_i\gamma_5\psi$ are called a_1 . The signal in these channels is not good. We only present data for those mass combinations where there is a ‘plateau’ over at least three time slices. Even in the best case the signal dies out by $t=14$, and so contamination from higher states is likely. We do not consider the data good enough to warrant further analysis.

The tables show in detail how all the masses are systematically lower for the WL correlators than for the SL or SS correlators. The effect is, however, less than 1σ for the pion and ρ . As discussed above, we take the results of Table IV as our best estimates.

To extrapolate the hadron masses towards the chiral limit

and to test the forms predicted by quenched chiral perturbation theory, we need to choose a definition of quark mass. We consider two possibilities. The first is the standard perturbative definition,

$$m_q^{\overline{\text{MS}}} = Z_m(1/2\kappa - 1/2\kappa_c), \quad (5.1)$$

while the second is nonperturbative [16],

$$-M_\pi \frac{\langle 0|A_4(t)J(0)|0\rangle}{\langle 0|P(t)J(0)|0\rangle} \xrightarrow{t \rightarrow \infty} \frac{Z_P}{Z_A} \frac{(m_{1,\text{np}} + m_{2,\text{np}})}{2}. \quad (5.2)$$

Here P and A_4 are local operators and J (which has the same Lorentz structure as either P or A_4) is constructed from the smeared Wuppertal source propagators. The data for the two

TABLE IV. Best estimates of meson masses [given by the average $(2WL + SL + SS)/4$ as explained in the text] at $\vec{p}=0$.

	π	A_4/A_4	A_4/π	π/A_4	ρ	a_0	a_1
CC	1.217(00)	1.217(01)	1.217(01)	1.217(01)	1.229(01)	1.426(07)	1.441(06)
CS	0.854(01)	0.854(01)	0.854(01)	0.854(01)	0.879(01)		1.113(08)
CU_1	0.814(01)	0.814(01)	0.814(01)	0.814(01)	0.842(01)		1.086(10)
CU_2	0.798(01)	0.799(01)	0.799(01)	0.799(01)	0.828(01)		1.081(12)
CU_3	0.789(01)	0.791(02)	0.790(01)	0.790(01)	0.819(02)		1.084(15)
SS	0.422(01)	0.422(01)	0.422(01)	0.422(01)	0.505(01)	0.727(12)	0.763(08)
SU_1	0.363(01)	0.363(01)	0.364(01)	0.363(01)	0.464(01)	0.700(16)	0.730(08)
SU_2	0.339(01)	0.339(01)	0.339(01)	0.338(01)	0.448(02)	0.718(21)	0.720(11)
SU_3	0.323(01)	0.323(01)	0.323(01)	0.323(01)	0.439(02)		0.720(12)
U_1U_1	0.296(01)	0.296(01)	0.297(01)	0.296(01)	0.422(02)	0.699(31)	0.694(10)
U_1U_2	0.267(01)	0.266(01)	0.267(01)	0.266(01)	0.405(02)		0.683(12)
U_1U_3	0.247(01)	0.247(01)	0.248(01)	0.246(01)	0.394(03)		0.682(15)
U_2U_2	0.234(01)	0.233(01)	0.234(01)	0.233(01)	0.387(03)		0.672(14)
U_2U_3	0.211(01)	0.210(01)	0.211(01)	0.210(01)	0.373(03)		0.669(17)
U_3U_3	0.185(01)	0.184(01)	0.186(01)	0.184(01)	0.361(05)		0.664(20)

choices of J are consistent, and so we use the average as the best estimate. We use tadpole-improved renormalization constants, defined by [17]

$$\begin{aligned} \frac{Z_m}{8\kappa_c} &= 1 - \alpha_{\overline{\text{MS}}}(q^*) \left(\frac{2}{\pi} \ln(\mu a) - 0.01 \right), \\ \sqrt{Z_\psi^1 Z_\psi^2} Z_A &= \sqrt{1 - 3\kappa_1/4\kappa_c} \sqrt{1 - 3\kappa_2/4\kappa_c} \\ &\quad \times [1 - 0.316\alpha_{\overline{\text{MS}}}(q^*)], \\ \sqrt{Z_\psi^1 Z_\psi^2} Z_P &= \sqrt{1 - 3\kappa_1/4\kappa_c} \sqrt{1 - 3\kappa_2/4\kappa_c} \\ &\quad \times \left(1 + \alpha_{\overline{\text{MS}}}(q^*) \left(\frac{2}{\pi} \ln(\mu a) - 1.0335 \right) \right). \end{aligned} \quad (5.3)$$

$Z_\psi^{1,2}$ are wave function renormalizations for the two quarks coupling to the bilinears, which have hopping parameters $\kappa_{1,2}$, respectively. The Z_ψ 's cancel in the ratio Z_P/Z_A . μ is the scale at which we match to the continuum renormalization scheme (here $\overline{\text{MS}}$), while q^* is a typical momentum in the one-loop integral. We choose $\mu=1/a$ and assume $q^*=1/a$. The masses can be run to other scales using the two-loop anomalous dimension relation [18]

$$\begin{aligned} \frac{m(Q)}{m(\mu)} &= \left(\frac{g^2(Q)}{g^2(\mu)} \right)^{\gamma_0/2\beta_0} \left[1 + \frac{g^2(Q) - g^2(\mu)}{16\pi^2} \right. \\ &\quad \left. \times \left(\frac{\gamma_1\beta_0 - \gamma_0\beta_1}{2\beta_0^2} \right) \right]. \end{aligned} \quad (5.4)$$

We mostly quote results for the scale $1/a$, but also give some results at scale 2 GeV, to allow comparison with other work.

It is important to note that, although we do not label m_{np} $\overline{\text{MS}}$ explicitly, both definitions yield estimates for the continuum mass in the $\overline{\text{MS}}$ scheme and should agree in the continuum limit. We give our results for both definitions in Table VII, below, and find a substantial difference between them. Most likely this is due to the failure of the perturbative expression for Z_P [18,11]. Details of this analysis will be presented elsewhere.

This difference is not, however, important for our study, since the two definitions of mass turn out to be proportional to very high accuracy for the six cases $\{U_i U_j\}$. This is shown in Fig. 4, in which we plot the average m_{np} of the quark and antiquark against the average value of $1/2\kappa$. The fit is given by $m_{\text{np}} = 0.867(4)(1/2\kappa) - 2.76(1)$. Thus, when extrapolating, it does not matter which definition of mass one uses. We choose to use m_{np} for most purposes in this paper—and we will drop the subscript henceforth. The perturbative mass, when it appears, will be distinguished by the superscript $\overline{\text{MS}}$.

We now consider extrapolations to the chiral limit. Figures 5 and 6 show, respectively, M_π^2 and M_ρ as a function of the average m_{np} . Only data from the combinations $\{U_i U_j\}$ (the six points with the smallest masses) and $\{SS, SU_j\}$ (the rightmost four points) are included.

We first consider linear fits to the data. These work well for the $\{U_i U_j\}$ points and are the fits shown in the figures. The fits give

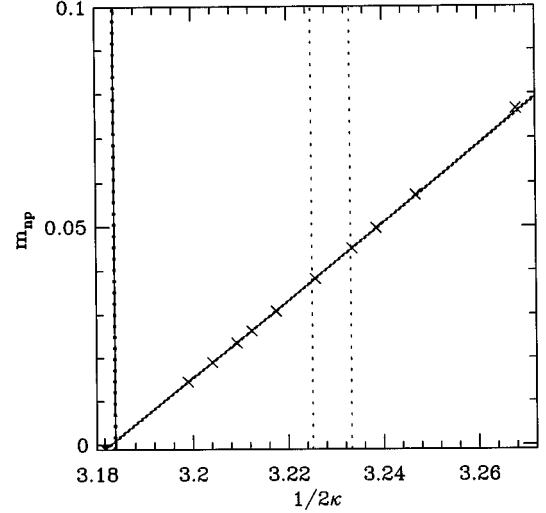


FIG. 4. Plot of data for m_{np} versus $1/2\kappa$. The linear fit is to the six $\{U_i U_j\}$ (lightest) points. The vertical lines show \bar{m} and the range of estimates of m_s .

$$\begin{aligned} M_\pi^2 &= a_\pi + c_\pi(m_1 + m_2) = 0.0013(5) \\ &\quad + 2.296(11)(m_1 + m_2)/2, \end{aligned} \quad (5.5)$$

$$M_\rho = a_\rho + c_\rho(m_1 + m_2) = 0.327(6) + 2.54(14)(m_1 + m_2)/2.$$

One interesting feature is that the pion intercept is slightly inconsistent with zero, whereas in the continuum limit of full QCD the intercept should vanish. This discrepancy could be due to discretization errors: For M_π^2 to be proportional to m_{np} , it must be true that $\langle 0|A_4|\pi\rangle \propto M_\pi$ [see Eq. (5.2)], which is guaranteed only in the continuum limit. A violation of this proportionality at $O(a)$ would lead to an additional term in Eq. (5.5) proportional to $\sqrt{am_{\text{np}}}$, where a is the lattice spacing. This could give rise to a nonzero intercept.

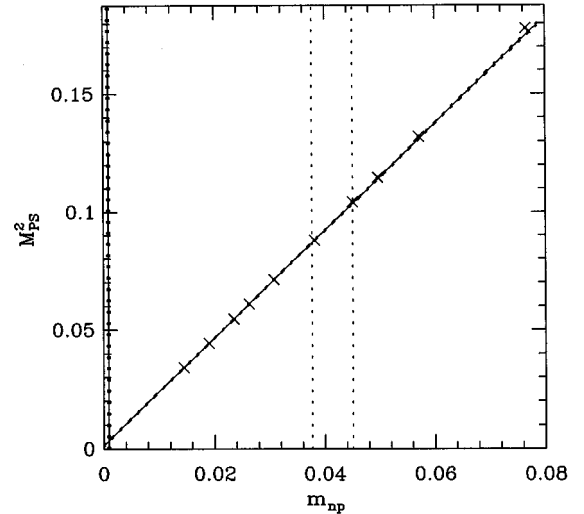


FIG. 5. M_π^2 versus m_{np} . The linear fit is to the six $\{U_i U_j\}$ points.

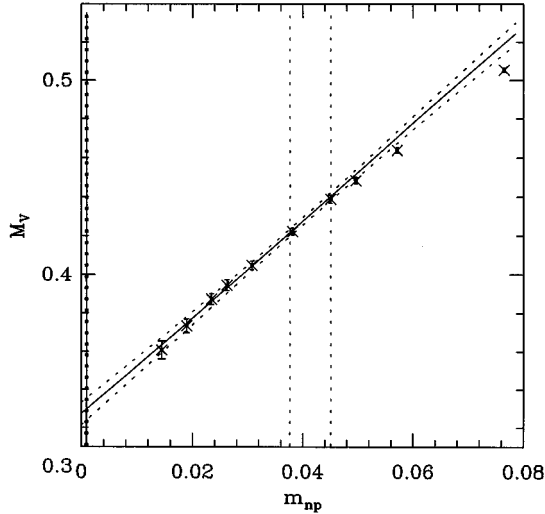


FIG. 6. M_ρ versus m_{np} . The linear fit is to the six $\{U_i U_j\}$ points.

Other possible culprits are quenched chiral logarithms—the terms proportional to δ in Eq. (4.1)—and finite size effects. We expect the latter to be insignificant, however, since $M_\pi L \geq 6$. Our data are not good enough to investigate this effect further. As a result of the nonzero intercept, the chiral limit (defined by $M_\pi = 0$) is at $m_{np}^{\text{chiral}} = -0.00058(21)$. In the following, when quoting quark masses in physical units we use $m_{np} - m_{np}^{\text{chiral}}$, i.e., we offset the zero of the mass scale. This offset is only significant for \bar{m} . When we use masses in lattice units, as we do in all our fits and extrapolations, we do not include this offset.

Using our linear fits we determine \bar{m}_{np} by extrapolating to the point where $M_K^2/M_\pi^2 = (137/768)^2$, finding $\bar{m}_{np} = 0.00093(21)$. The resulting value of $M_\rho a$ gives us an estimate of the scale

$$a^{-1}(M_\rho) = 2.3301(41) \text{ GeV}. \quad (5.6)$$

Using this value and including the offset in the mass scale, we find $\bar{m}(1/a) = 3.51(6) \text{ MeV}$ [$\bar{m}(2 \text{ GeV}) = 3.60(5) \text{ MeV}$]. To facilitate comparison with earlier calculations, it is useful to give results for the critical and light quark hopping parameters. Using linear fits versus $1/\kappa$, we find

$$\kappa_c = 0.157131(9), \quad \kappa_l = 0.157046(9). \quad (5.7)$$

We note that linear fits work well for the subsample $\{SS, SU_j\}$ (and for $\{CU_j\}$, not shown in the figures) as well, and we use them below when calculating the masses of strange and charm mesons.

The figures show that linear fits are inadequate for the combined $\{U_i U_j\}$ and $\{SS, SU_j\}$ data. This is particularly striking for M_ρ , where there is a definite negative curvature, which, if ignored, could lead to an overestimate of a_ρ . Thus we have tried fits to the combined data involving higher order terms in the chiral expansion. A quadratic fit to M_π^2 works well, but has little impact on extrapolations, increasing a_π by about 1σ . For the ρ , motivated by chiral perturbation theory, we have used two forms of higher order terms:

TABLE V. Estimates of the strange quark mass obtained by matching different quantities with their physical values. Results are given for (1) κ_s , (2) the lattice nonperturbative mass m_{np}/a evaluated at 1/a and 2 GeV, and (3) the lattice perturbative mass m_s^{MS} evaluated at 2 GeV. The latter three masses are in MeV.

Quantity	κ_s	$m_{s,np}(1/a)$	$m_{s,np}(2 \text{ GeV})$	$m_s^{\text{MS}}(2 \text{ GeV})$
M_K^2/M_π^2	0.15503(7)	87(2)	89(2)	129(2)
M_{K^*}/M_ρ	0.15479(19)	98(7)	100(7)	145(9)
M_ϕ/M_ρ	0.15464(17)	104(6)	106(6)	154(8)

$$M_\rho = a_\rho + c_\rho(m_1 + m_2) + d_\rho(m_1 + m_2)^{3/2}, \quad (5.8)$$

$$M_\rho = a_\rho + c_\rho(m_1 + m_2) + e_\rho(m_1 + m_2)^2.$$

These fits, when extrapolated to \bar{m} (calculated self-consistently), yield smaller values of $M_\rho(\bar{m})$ and thus larger scales than the linear fit:

$$a^{-1}(M_\rho) = 2.365(48) \text{ GeV} \quad (m^{3/4} \text{ fit}), \quad (5.9)$$

$$a^{-1}(M_\rho) = 2.344(42) \text{ GeV} \quad (m^2 \text{ fit}).$$

The difference from the result of the linear fit is, however, within the statistical errors. Our data are good enough to see the curvature, but not precise enough to study it in detail. In particular, we cannot distinguish between the two forms in Eq. (5.8), both doing a good job of fitting the combined $\{U_i U_j\}$ and $\{SS, SU_j\}$ data sets. In view of this, we chose to use the scale from the linear fit for most of our subsequent analysis. For comparison, we note that the scale we find from f_π is 2265(57) MeV [19], while the NRQCD Collaboration reports a value 2.4(1) GeV from a mean of charmonium and Y spectroscopy [20]. Thus different estimates based on meson correlators are consistent. In the remainder of the paper we shall take the scale from M_ρ and assign a 3% systematic uncertainty to cover the spread in a^{-1} obtained from different mesonic observables and different types of extrapolations.

Using the linear fits defined in Eq. (5.5), we determine the lattice strange quark mass by first extrapolating M_K^2/M_π^2 , M_{K^*}/M_ρ , or M_ϕ/M_ρ to \bar{m} and then linearly interpolating between U_1 and S until these quantities match their physical values. (We use $M_K = 495 \text{ MeV}$, $M_{K^*} = 894 \text{ MeV}$, and $M_\phi = 1019 \text{ MeV}$). The results are given in Table V in terms of κ and the two definitions of quark mass discussed above, except that we have here run the masses to a scale of 2 GeV to facilitate comparison with other work.

The three ratios lead to significantly different results for m_s , presumably because of a combination of quenching and discretization errors. Using M_K^2/M_π^2 to fix m_s implies $m_s \equiv 25\bar{m}$, since we use the lowest order chiral expansion to fit the data. On the other hand, the estimates using M_ϕ/M_ρ and M_{K^*}/M_ρ are not constrained by the chiral expansion and give $m_s/\bar{m} \approx 30$, in surprisingly good agreement with the next-to-leading chiral result [21]. In this paper we quote all results using $m_s(M_\phi)$.

Recently Lacock and Michael [22] suggested using the dimensionless quantity $J_V = M_V \partial M_V / \partial M_\pi^2$ to test the quenched approximation. Using a linear fit, we find

TABLE VI. Pseudoscalar (first set) and vector (second set) meson energies as a function of momentum. The data are the average of SL and SS estimates.

	$p^2=1$	$p^2=2$	$p^2=3$	$p^2=4$	$p^2=1$	$p^2=2$	$p^2=3$	$p^2=4$
CC	1.231(01)	1.244(01)	1.255(02)	1.268(01)	1.243(01)	1.255(01)	1.267(02)	1.278(02)
CS	0.874(01)	0.893(02)	0.913(03)	0.930(02)	0.899(01)	0.917(02)	0.937(03)	0.951(03)
CU_1	0.836(02)	0.855(02)	0.876(03)	0.895(02)	0.863(02)	0.881(02)	0.901(03)	0.917(04)
CU_2	0.821(02)	0.841(02)	0.861(04)	0.881(03)	0.849(02)	0.868(03)	0.888(04)	0.905(04)
CU_3	0.814(03)	0.833(03)	0.853(04)	0.873(03)	0.841(03)	0.860(04)	0.882(04)	0.898(05)
SS	0.466(01)	0.504(02)	0.547(04)	0.578(04)	0.541(02)	0.575(03)	0.614(05)	0.642(04)
SU_1	0.414(02)	0.456(03)	0.505(06)	0.539(04)	0.503(03)	0.540(03)	0.583(06)	0.613(05)
SU_2	0.393(02)	0.438(03)	0.487(07)	0.522(05)	0.489(03)	0.528(04)	0.571(07)	0.602(06)
SU_3	0.380(02)	0.427(03)	0.474(08)	0.511(06)	0.482(04)	0.522(05)	0.565(90)	0.596(07)
U_1U_1	0.357(02)	0.406(03)	0.460(08)	0.497(06)	0.465(04)	0.508(05)	0.553(08)	0.583(06)
U_1U_2	0.333(02)	0.386(03)	0.438(09)	0.480(07)	0.452(05)	0.496(06)	0.541(10)	0.572(07)
U_1U_3	0.317(02)	0.372(04)	0.423(11)	0.469(08)	0.445(06)	0.490(07)	0.534(12)	0.566(08)
U_2U_3	0.307(02)	0.363(04)	0.416(11)	0.464(09)	0.439(06)	0.484(08)	0.529(12)	0.561(09)
U_2U_3	0.290(03)	0.349(05)	0.399(13)	0.454(11)	0.432(08)	0.478(10)	0.520(15)	0.554(10)
U_3U_3	0.272(03)	0.333(05)	0.379(16)	0.445(13)	0.424(10)	0.471(13)	0.509(19)	0.546(13)

$$J_{K^*} = 0.41(1), \quad J_\rho = 0.36(1), \quad (5.10)$$

to be compared to the experimental values of ≈ 0.48 and ≈ 0.41 , respectively. Again, the discrepancy is presumably due to a combination of discretization and quenching errors.

VI. $O(ma)$ DISCRETIZATION ERRORS

At $\beta=6$, the charm mass is such that $m_c a \sim 1$, and so there are potentially large $O(m_c a)$ discretization errors in all quantities involving charm quarks. These are in addition to errors of $O(\Lambda_{\text{QCD}} a)$, which are common to all quantities. One effect of $O(a)$ errors is that there is a difference between the ‘‘static’’ mass $M_1 = E(\vec{p}=0)$ and the ‘‘kinetic’’ mass $M_2 = (\partial^2 E / \partial p^2|_{p=0})^{-1}$. Here the energy is determined from the rate of exponential decay of the correlator, $C(t) \propto \exp[-E(\vec{p})t]$. M_1 and M_2 agree in the continuum limit, whatever the mass of the state.

To evaluate M_2 , we have tested four forms of dispersion relation:

$$\begin{aligned} \text{(A)} \quad E^2 &= p^2 + M^2 \Rightarrow M_2 = M, \\ \text{(B)} \quad \sinh^2 E &= \sin^2 p + \sinh^2 M \Rightarrow M_2 = \frac{1}{2} \sinh 2M, \\ \text{(C)} \quad \sinh^2 \frac{E}{2} &= \sin^2 \frac{p}{2} + \sinh^2 \frac{M}{2} \Rightarrow M_2 = \sinh M, \\ \text{(D)} \quad \sinh^2 \frac{E}{4} &= \sin^2 \frac{p}{4} + \sinh^2 \frac{M}{4} \Rightarrow M_2 = 2 \sinh \frac{M}{2}. \end{aligned} \quad (6.1)$$

(A) is the continuum relation, while (B), (C), and (D) are lattice forms following from different choices of lattice action. In particular, (C) follows from the nearest neighbor symmetric difference discretization of the action for a scalar. Our results for $E(\vec{p})$ are collected in Table VI, and in Fig. 7 we show how the various dispersion relations fare for the CU_1 meson. For all heavy-heavy and heavy-light mesons, our results turn out to be consistent with dispersion relation (C), but not with the other forms.

Using this result, we have that $M_2 = \sinh M_1$. In Table VII we compare M_1 and M_2 for the pseudoscalar and vector mesons. The difference is tiny for the smallest quark masses, but substantial for charmed mesons. Our results for charmed meson masses (obtained by linear extrapolation in the light quark mass and with m_c chosen to be $\kappa=0.135$) are given in Table VIII. There is a significant difference between the estimates using M_1 and M_2 : For the D mesons the difference is $\sim 10\%$, while for the charmonium system it is $25\text{--}30\%$. This suggests that $O(ma)$ corrections in the Wilson action are already large in the charm region. This is also apparent from the mass splittings—the spin-spin and spin-orbit interactions are underestimated by the Wilson action, as has been previously observed [23].

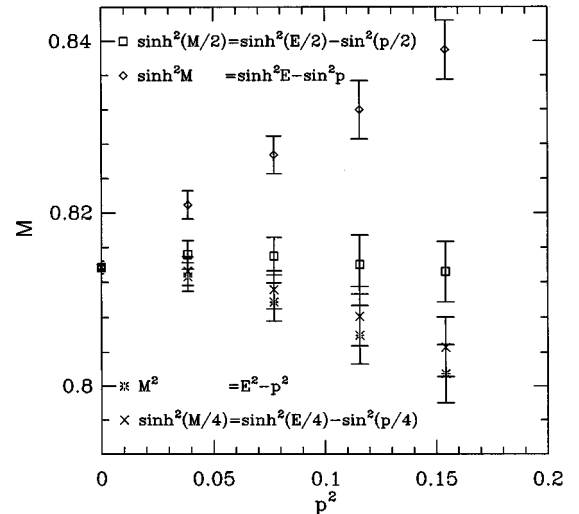


FIG. 7. Test of four lattice dispersion relations [see Eq. (6.1)] using the lattice pion data at various momenta for the case CU_1 . The data favor the nearest-neighbor symmetric-difference relativistic dispersion relation $\sinh^2(E/2) - \sin^2(p/2) = \sinh^2(M/2)$, as shown by the square symbols.

TABLE VII. Comparison of $M_1 = E(\vec{p}=0)$ and $M_2 = \sinh M_1$. We also give the values of the average nonperturbative m_{np} and perturbative definitions of the quark mass in the $\overline{\text{MS}}$ scheme as defined in Eqs. (5.2) and (5.3). Both are in lattice units, evaluated at the scale $1/a$.

State	M_π		M_ρ		m_{np}	m_q
	M_1	M_2	M_1	M_2		
CC	1.217(0)	1.541(1)	1.229(1)	1.564(2)	0.4569(2)	0.6563(2)
CS	0.854(1)	0.962(1)	0.879(1)	0.999(2)	0.2625(2)	0.3822(2)
CU_1	0.814(1)	0.908(2)	0.842(1)	0.947(2)	0.2419(3)	0.3557(2)
CU_2	0.799(1)	0.888(2)	0.828(1)	0.927(3)	0.2339(3)	0.3453(2)
CU_3	0.790(1)	0.877(3)	0.819(2)	0.916(4)	0.2291(4)	0.3388(2)
SS	0.422(1)	0.435(1)	0.505(1)	0.528(2)	0.0756(2)	0.1081(2)
SU_1	0.363(1)	0.372(1)	0.464(1)	0.481(3)	0.0565(2)	0.0816(2)
SU_2	0.339(1)	0.346(1)	0.448(2)	0.465(3)	0.0490(2)	0.0711(2)
SU_3	0.323(1)	0.330(1)	0.439(2)	0.454(4)	0.0445(2)	0.0647(2)
U_1U_1	0.296(1)	0.301(1)	0.422(2)	0.436(3)	0.0377(2)	0.0550(2)
U_1U_2	0.267(1)	0.271(1)	0.405(2)	0.417(4)	0.0304(2)	0.0446(2)
U_1U_3	0.247(1)	0.250(1)	0.394(3)	0.406(5)	0.0259(2)	0.0382(2)
U_2U_2	0.234(1)	0.236(1)	0.387(3)	0.398(5)	0.0232(2)	0.0342(2)
U_2U_3	0.211(1)	0.213(1)	0.373(3)	0.385(7)	0.0187(2)	0.0277(2)
U_3U_3	0.185(1)	0.186(1)	0.361(5)	0.370(9)	0.0143(2)	0.0213(2)

VII. BARYON MASSES

Our baryon mass analysis is based on two overlapping data sets. For the complete data set (170 configurations), we have results for only WL and SL correlators and for only a subset of possible quark combinations. On the last 110 configurations we also calculate SS correlators and use all degenerate and nondegenerate combinations made up of S and U_i quarks. Our results for the masses are given in Tables IX, X, and XI. The sample size is indicated by the subscript in the table headings. In the following, some analyses are only possible on the smaller sample, and we label such results by an asterisk next to the error estimate.

TABLE VIII. Comparison of lattice estimates of D meson and charmonium masses with the experimental data. We show results for M_1 and M_2 and for the two different ways of setting m_s described in the text.

	D meson masses in MeV		
	M_1	M_2	Expt.
M_D	1805(31)	1990(34)	1869
M_{D^*}	1876(32)	2085(35)	2008
$M_{D_s^*}[m_s(M_K)]$	1896(30)	2112(32)	1969
$M_{D_s^*}[m_s(M_\phi)]$	1914(26)	2137(27)	1969
$M_{D_s^*}[m_s(M_K)]$	1961(31)	2201(34)	2110?
$M_{D_s^*}[m_s(M_\phi)]$	1978(27)	2224(29)	2110?
$M_{\eta_c^3}(^1S_0)$	2836(50)	3590(64)	2980
$M_{J/\psi}(^3S_1)$	2865(51)	3643(65)	3097
$M_{\chi_{c0}}(^3P_0)$	3324(60)	4572(86)	3415
$M_{\chi_{c1}}(^3P_1)$	3357(60)	4646(86)	3510
$\Delta M(^3S_1-^1S_0)$	29(1)	53(2)	117
$\Delta M(^3P_1-^3P_0)$	33(9)	74(18)	95
$\Delta M(^3P_0-^3S_1)$	459(17)	929(36)	318

A. Correlators

It is necessary to introduce some notation to explain the correlation functions we calculate. We adapt that used in quenched chiral perturbation theory for baryons [14]. Assume that we have three flavors of quark, labeled by u , d , and s . To create spin-1/2 baryons we can use the interpolating operators

$$\mathcal{O}_{(ij)k} = (\psi_{a,i}^T C \gamma_5 \psi_{b,j}) \psi_{c,k} \epsilon^{abc}, \quad (7.1)$$

where a , b , and c label color, while i , j , and k label flavor. It is simple to show that $\mathcal{O}_{(ij)k} = -\mathcal{O}_{(ji)k}$, so that there are only nine independent operators, eight SU(3) octets and the singlet $\sum_{ijk} \epsilon^{ijk} \mathcal{O}_{ijk}$. One way to project against the singlet is to form

$$\mathcal{B}_{ijk} = \mathcal{O}_{(ij)k} + \mathcal{O}_{(ik)j} = \mathcal{B}_{ikj}. \quad (7.2)$$

There are eight independent \mathcal{B}_{ijk} 's, the relation to the usual states being exemplified by

$$\begin{aligned} \sqrt{2}p &= -\mathcal{B}_{duu} = 2\mathcal{B}_{uud} = 2\mathcal{B}_{udu}, \\ \sqrt{2}\Sigma^+ &= -\mathcal{B}_{suu} = 2\mathcal{B}_{uus} = 2\mathcal{B}_{usu}, \\ \Sigma^0 &= \mathcal{B}_{uds} + \mathcal{B}_{dsu} = -\mathcal{B}_{sud}, \\ \sqrt{3}\Lambda^0 &= \mathcal{B}_{uds} - \mathcal{B}_{dsu}. \end{aligned} \quad (7.3)$$

The overall factor in these equations is arbitrary, while the relative normalization is fixed by SU(3) symmetry.

All spin-1/2 baryon correlators are built out of the two contractions shown in Fig. 8. The notation $\langle DU \rangle S = \langle UD \rangle S$ corresponds to quarks of flavors U and D contracted into a closed loop, while the propagator for S carries the spin quantum numbers of the baryon. The notation (DUS) corresponds to a single ordered contraction of the three quarks.

TABLE IX. Mass estimates for Λ -like baryons.

	WL_{110}	SL_{110}	SS_{110}	AV_{110}
$S[SS]$	0.786(03)	0.791(04)	0.793(04)	0.789(02)
$S[SU_1]$	0.734(04)	0.740(04)	0.742(04)	0.738(02)
$S[SU_2]$	0.712(04)	0.720(04)	0.721(04)	0.716(03)
$S[SU_3]$	0.698(04)	0.707(05)	0.708(04)	0.703(03)
$S[U_1U_1]$	0.678(04)	0.687(04)	0.688(04)	0.683(03)
$S[U_1U_2]$	0.655(04)	0.665(05)	0.665(04)	0.660(03)
$S[U_1U_3]$	0.640(05)	0.652(05)	0.651(05)	0.646(03)
$S[U_2U_2]$	0.630(05)	0.642(05)	0.642(05)	0.636(03)
$S[U_2U_3]$	0.614(06)	0.627(06)	0.627(05)	0.620(04)
$S[U_3U_3]$	0.597(07)	0.611(07)	0.610(06)	0.604(04)
$U_1[SS]$	0.740(04)	0.747(04)	0.749(04)	0.744(03)
$U_1[SU_1]$	0.687(05)	0.696(05)	0.697(04)	0.691(03)
$U_1[SU_2]$	0.663(04)	0.675(05)	0.675(05)	0.669(03)
$U_1[SU_3]$	0.648(05)	0.661(05)	0.661(05)	0.655(03)
$U_1[U_1U_1]$	0.630(05)	0.643(05)	0.642(05)	0.636(03)
$U_1[U_1U_2]$	0.605(05)	0.620(06)	0.619(05)	0.612(03)
$U_1[U_1U_3]$	0.589(06)	0.605(06)	0.604(06)	0.597(04)
$U_1[U_2U_2]$	0.579(06)	0.596(06)	0.595(06)	0.587(04)
$U_1[U_2U_3]$	0.562(07)	0.580(07)	0.579(06)	0.571(04)
$U_1[U_3U_3]$	0.544(08)	0.563(09)	0.562(07)	0.553(05)
$U_2[SS]$	0.723(04)	0.731(05)	0.732(04)	0.727(03)
$U_2[SU_1]$	0.668(05)	0.679(05)	0.679(05)	0.674(03)
$U_2[SU_2]$	0.643(05)	0.657(06)	0.657(05)	0.650(03)
$U_2[SU_3]$	0.627(06)	0.643(06)	0.643(06)	0.635(04)
$U_2[U_1U_1]$	0.610(06)	0.626(06)	0.625(05)	0.617(04)
$U_2[U_1U_2]$	0.584(06)	0.602(07)	0.601(06)	0.593(04)
$U_2[U_1U_3]$	0.567(07)	0.587(08)	0.586(07)	0.577(05)
$U_2[U_2U_2]$	0.557(07)	0.578(08)	0.577(07)	0.567(05)
$U_2[U_2U_3]$	0.539(08)	0.561(09)	0.560(08)	0.550(05)
$U_2[U_3U_3]$	0.520(10)	0.543(11)	0.543(09)	0.532(06)
$U_3[SS]$	0.712(05)	0.722(05)	0.723(05)	0.717(03)
$U_3[SU_1]$	0.656(06)	0.670(06)	0.669(05)	0.663(04)
$U_3[SU_2]$	0.631(06)	0.647(07)	0.646(06)	0.639(04)
$U_3[SU_3]$	0.614(07)	0.632(08)	0.631(07)	0.623(04)
$U_3[U_1U_1]$	0.598(06)	0.616(07)	0.615(06)	0.607(04)
$U_3[U_1U_2]$	0.572(07)	0.592(08)	0.590(07)	0.581(05)
$U_3[U_1U_3]$	0.554(08)	0.576(09)	0.574(08)	0.564(05)
$U_3[U_2U_2]$	0.544(08)	0.567(09)	0.565(08)	0.555(05)
$U_3[U_2U_3]$	0.525(09)	0.550(11)	0.549(09)	0.537(06)
$U_3[U_3U_3]$	0.506(11)	0.531(13)	0.531(10)	0.518(07)

We consider two types of correlator, “ Σ like” and “ Λ like.” The former is exemplified by that of the Σ^0 ,

$$S\{UD\} = S\{DU\} \equiv \langle \mathcal{B}_{sud}(x) \overline{\mathcal{B}_{sud}(0)} \rangle \\ = \langle US \rangle D + \langle DS \rangle U + (USD) + (DSU). \quad (7.4)$$

(This equation defines our sign conventions for the contractions.) The proton, neutron, Σ^+ , Σ^- , Ξ^0 , and Ξ^- correlators are also of this type: They are, respectively, $D\{UU\}$, $U\{DD\}$, $S\{UU\}$, $S\{DD\}$, $U\{SS\}$, and $D\{SS\}$. The second type of correlator is that of the Λ^0

$$S\{UD\} = S\{DU\} \equiv (1/3)[\langle US \rangle D + \langle DS \rangle U + 4\langle UD \rangle S \\ - (USD) - (DSU) + 2(SUD) + 2(SDU) \\ + 2(UDS) + 2(DUS)]. \quad (7.5)$$

When $m_u \neq m_d$, there is also a nonvanishing $\Lambda^0 - \Sigma^0$ cross correlator, but we have not found this to give useful results.

We have calculated the two types of spin-1/2 baryon correlator for all independent mass combinations involving U_i and S quarks. The results are given in Tables IX and X, respectively. Masses from correlators of the form $A[AB]$ and $A\{AB\}$ are also included even though they are not independent—the correlators are related by

$$A[AB] = \frac{1}{4}(3B[AA] + B\{AA\}), \quad (7.6)$$

$$A\{AB\} = \frac{1}{4}(B[AA] + 3B\{AA\}).$$

One can think of the results for the $A\{BB\}$ and $A[BB]$ masses as being those for the Σ and Λ , respectively, with $m_s = m_A$ and $m_u = m_d = m_B$. Unlike in the real world, there is nothing to stop these two masses being the same, i.e., $m_A = m_B$, in the quenched approximation. Note, however, that in this case the Σ and Λ are also degenerate, i.e., $M(A\{AA\}) = M(A[AA])$. Indeed, the contractions in the two cases are identical.

The interpretation of the results for the completely non-degenerate correlators $A[BC]$ and $A\{BC\}$ is more complicated. Because isospin is broken, the Σ^0 - and Λ -like states mix, with both correlators containing contributions from both physical states. Let M_+ and M_- be the masses of the heavier and lighter states, respectively, and δM the mass difference. At long times, the effective mass for both correlators will asymptote to M_- . However, at times short compared to the inverse mass difference, i.e., $\delta M t_{\max} \ll 1$, there will be an approximate plateau at a value which is a weighted average of the two masses. To see this, we pick the Λ correlator and write it as

$$C_\Lambda(t) = A e^{-M_- t} (\cos^2 \theta + \sin^2 \theta e^{-\delta M t}) + \dots, \quad (7.7)$$

where $\tan \theta$ is the ratio of the amplitudes to create the two mixed states and the ellipsis represents excited states. The effective mass is

$$m(\Lambda)_{\text{eff}}(t) = - \frac{d \ln C_\Lambda(t)}{dt} = M_- + \sin^2 \theta \delta M \\ \times [1 + O(\delta M t)] \approx \cos^2 \theta M_- + \sin^2 \theta M_+. \quad (7.8)$$

Thus the effective mass is almost constant, and given our errors, we cannot distinguish it from a plateau. We discuss below the interpretation of the resulting “mass.”

We have also calculated the masses of spin-3/2 baryons. Here there is only one type of operator, which is completely symmetric in flavor. Our results for all 20 mass combinations built out of U_i and S quarks are given in Table XI.

TABLE X. Mass estimates for Σ -like baryons.

	WL_{110}	SL_{110}	SS_{110}	AV_{110}	WL_{170}	SL_{170}	AV_{170}
$S\{SS\}$	0.786(03)	0.791(04)	0.793(04)	0.789(02)	0.786(03)	0.794(03)	0.790(02)
$S\{SU_1\}$	0.738(04)	0.745(04)	0.746(04)	0.742(03)			
$S\{SU_2\}$	0.718(04)	0.727(04)	0.728(04)	0.723(03)			
$S\{SU_3\}$	0.706(04)	0.716(05)	0.717(05)	0.711(03)			
$S\{U_1U_1\}$	0.689(04)	0.699(05)	0.700(04)	0.695(03)	0.689(04)	0.702(04)	0.695(03)
$S\{U_1U_2\}$	0.669(05)	0.682(05)	0.682(05)	0.676(03)			
$S\{U_1U_3\}$	0.657(05)	0.672(06)	0.671(05)	0.664(04)			
$S\{U_2U_2\}$	0.649(06)	0.665(06)	0.664(06)	0.657(04)	0.649(04)	0.667(05)	0.658(03)
$S\{U_2U_3\}$	0.636(07)	0.654(07)	0.654(06)	0.645(04)			
$S\{U_3U_3\}$	0.622(08)	0.644(09)	0.643(08)	0.633(05)	0.625(06)	0.647(07)	0.636(04)
$U_1\{SS\}$	0.732(04)	0.738(04)	0.739(04)	0.736(02)	0.732(03)	0.744(04)	0.738(02)
$U_1\{SU_1\}$	0.681(05)	0.690(04)	0.690(04)	0.686(03)			
$U_1\{SU_2\}$	0.659(04)	0.671(05)	0.671(04)	0.665(03)			
$U_1\{SU_3\}$	0.646(05)	0.659(05)	0.658(05)	0.652(03)			
$U_1\{U_1U_1\}$	0.630(05)	0.643(05)	0.642(05)	0.636(03)	0.630(05)	0.645(05)	0.638(03)
$U_1\{U_1U_2\}$	0.608(05)	0.624(06)	0.623(05)	0.616(04)			
$U_1\{U_1U_3\}$	0.594(06)	0.612(07)	0.611(06)	0.603(04)			
$U_1\{U_2U_2\}$	0.586(06)	0.605(07)	0.604(06)	0.595(04)	0.588(05)	0.607(06)	0.598(04)
$U_1\{U_2U_3\}$	0.572(07)	0.593(08)	0.592(07)	0.582(05)			
$U_1\{U_3U_3\}$	0.557(09)	0.581(10)	0.580(08)	0.569(06)	0.562(07)	0.583(08)	0.573(05)
$U_2\{SS\}$	0.710(04)	0.717(04)	0.718(04)	0.714(03)	0.708(04)	0.720(04)	0.714(03)
$U_2\{SU_1\}$	0.657(05)	0.667(05)	0.667(04)	0.662(03)			
$U_2\{SU_2\}$	0.634(05)	0.646(05)	0.646(05)	0.640(03)			
$U_2\{SU_3\}$	0.619(06)	0.633(06)	0.633(05)	0.626(04)			
$U_2\{U_1U_1\}$	0.603(05)	0.618(06)	0.618(05)	0.611(03)	0.605(06)	0.621(06)	0.613(03)
$U_2\{U_1U_2\}$	0.580(06)	0.598(07)	0.597(06)	0.589(04)			
$U_2\{U_1U_3\}$	0.565(07)	0.585(08)	0.584(06)	0.575(04)			
$U_2\{U_2U_2\}$	0.557(07)	0.578(08)	0.577(07)	0.567(05)	0.561(06)	0.581(07)	0.571(04)
$U_2\{U_2U_3\}$	0.542(08)	0.565(09)	0.564(08)	0.553(05)			
$U_2\{U_3U_3\}$	0.526(10)	0.552(11)	0.551(09)	0.538(06)	0.534(08)	0.555(09)	0.544(06)
$U_3\{SS\}$	0.696(05)	0.704(05)	0.704(04)	0.700(03)	0.694(04)	0.708(05)	0.701(03)
$U_3\{SU_1\}$	0.642(06)	0.653(05)	0.652(05)	0.647(03)			
$U_3\{SU_2\}$	0.617(06)	0.631(06)	0.630(05)	0.624(04)			
$U_3\{SU_3\}$	0.602(07)	0.616(07)	0.616(06)	0.609(04)			
$U_3\{U_1U_1\}$	0.586(06)	0.602(06)	0.602(06)	0.594(04)	0.589(06)	0.606(06)	0.597(04)
$U_3\{U_1U_2\}$	0.563(07)	0.581(08)	0.580(06)	0.572(04)			
$U_3\{U_1U_3\}$	0.547(08)	0.567(09)	0.566(07)	0.557(05)			
$U_3\{U_2U_2\}$	0.539(08)	0.560(09)	0.559(07)	0.549(05)	0.543(08)	0.564(08)	0.553(05)
$U_3\{U_2U_3\}$	0.523(09)	0.545(11)	0.545(09)	0.534(06)			
$U_3\{U_3U_3\}$	0.506(11)	0.531(13)	0.531(10)	0.518(07)	0.515(10)	0.536(10)	0.525(07)

We analyze the baryon masses using the chiral expansion. We first consider the spin-1/2 baryons, returning to spin-3/2 baryons later in this section. We couch the discussion in terms similar to those used in full QCD. If we keep only constants and terms linear in quark masses (and drop nonanalytic terms of the form $\delta m_q^{1/2}$ as discussed in Sec. IV), then it is straightforward to show, using quenched chiral perturbation theory [14], that

$$M(\Sigma^+) = M(S\{UU\}) = M_0 + 4Fm_u + 2(F - D)m_s, \quad (7.9)$$

$$M(\Lambda) = M(S[UU]) = M_0 + 4\left(F - \frac{2D}{3}\right)m_u + 2\left(F + \frac{D}{3}\right)m_s.$$

Here M_0 is spin-1/2 baryon mass in the chiral limit and F and D are the usual reduced matrix elements of scalar densities. Note that there is no dependence on m_d , since the d quark does not enter the correlators. These results can also be obtained using mass perturbation theory in full QCD and then deleting terms proportional to $m_u + m_d + m_s$, which correspond to contributions from internal quark loops. We stress that these formulas apply to all the states we consider—for example, the proton mass is $M(D\{UU\})$ and is obtained by replacing m_s with m_d in the formula for $M(\Sigma^+)$.

At this order in the chiral expansion, it is simple to extend the results to baryons composed of three nondegenerate quarks. The mass matrix in the $(\Sigma^0, \Lambda) = (S\{UD\}, S[UD])$ basis is

$$\begin{pmatrix} \alpha & \lambda \\ \gamma & \beta \end{pmatrix} = \begin{pmatrix} M_0 + 4F\bar{m} + 2(F-D)m_s & \frac{2D}{\sqrt{3}}(m_u - m_d) \\ \frac{2D}{\sqrt{3}}(m_u - m_d) & M_0 + 4\left(F - \frac{2D}{3}\right)\bar{m} + 2\left(F + \frac{D}{3}\right)m_s \end{pmatrix}. \quad (7.10)$$

Diagonalizing this matrix gives the eigenvalues M_{\pm} with a mixing angle θ . If we assume that the same mixing angle applies for the interpolating fields, which we think is true up to corrections of $O(m_q^{3/2})$, then θ is the angle appearing in our previous expressions for the Λ correlator [Eq. (7.7)]. The ‘‘short-time effective mass,’’ Eq. (7.8), is then

$$M(\Lambda)_{\text{eff}} \approx \cos^2 \theta M_- + \sin^2 \theta M_+ = \beta. \quad (7.11)$$

A similar argument shows that

$$M(\Sigma)_{\text{eff}} \approx \sin^2 \theta M_- + \cos^2 \theta M_+ = \alpha. \quad (7.12)$$

Thus we find the surprising result that the short-time effective masses are insensitive to the isospin breaking term γ . Furthermore, the expressions for α and β are exactly the same as the formulas applicable when isospin is unbroken, Eqs. (7.9), except that m_u is replaced by the average mass \bar{m} .

We have not extended this analysis to higher order in the chiral expansion. Nevertheless, we use it as motivation for including our results for baryons composed of completely nondegenerate quarks by assuming that the effective masses satisfy

$$M(A\{BC\}) = M(A\{DD\}), \quad M(A[BC]) = M(A[DD]), \quad (7.13)$$

where $m_D = (m_B + m_C)/2$. We make clear in the following where we are using this assumption and where not.

A large part of our analysis concerns mass splittings between, for example, spin-1/2 baryons. In most cases, we have extracted these differences by directly fitting to the ratio of the appropriate correlators. Thus, for example,

$$\frac{\Gamma_{\Sigma}(t)}{\Gamma_N(t)} \sim e^{-(M_{\Sigma} - M_N)t},$$

and so the mass difference is obtained from a single fit. This has the advantage of both reducing some of the systematic errors (e.g., those arising from excited state contamination) and of improving the statistical errors. We find that estimates obtained in this manner are consistent with those obtained from individual fits, but have errors which are 3–5 times smaller.

B. Spin-1/2 baryon mass splittings

In this subsection we use our results for mass splittings between spin-1/2 baryons to extract predictions for the physical mass splittings and to study the chiral behavior of baryon masses. It turns out that the leading chiral prediction, Eq. (7.9), gives a poor description of our data. Higher order terms are essential in order to extrapolate reliably from our quark masses and have a significant impact on the final re-

TABLE XI. Mass estimates for the decuplet baryons.

	WL_{110}	SL_{110}	SS_{110}	AV_{110}	WL_{170}	SL_{170}	AV_{170}
$\{SSS\}$	0.832(05)	0.843(06)	0.843(07)	0.837(04)	0.831(04)	0.845(05)	0.838(03)
$\{SSU_1\}$	0.788(06)	0.803(07)	0.802(07)	0.795(05)			
$\{SSU_2\}$	0.770(07)	0.789(07)	0.786(08)	0.779(06)			
$\{SSU_3\}$	0.760(08)	0.781(09)	0.778(08)	0.770(06)			
$\{SU_1U_1\}$	0.744(08)	0.764(08)	0.761(08)	0.753(06)			
$\{SU_1U_2\}$	0.725(10)	0.750(09)	0.747(08)	0.736(07)			
$\{SU_1U_3\}$	0.710(11)	0.741(11)	0.738(09)	0.725(08)			
$\{SU_2U_2\}$	0.705(10)	0.736(11)	0.732(09)	0.719(07)			
$\{SU_2U_3\}$	0.690(11)	0.727(13)	0.724(10)	0.708(08)			
$\{SU_3U_3\}$	0.674(09)	0.718(15)	0.716(11)	0.696(08)			
$\{U_1U_1U_1\}$	0.697(08)	0.726(10)	0.721(09)	0.710(06)	0.699(08)	0.721(09)	0.710(06)
$\{U_1U_1U_2\}$	0.677(09)	0.712(12)	0.706(10)	0.693(07)			
$\{U_1U_1U_3\}$	0.663(11)	0.704(14)	0.699(11)	0.682(08)			
$\{U_1U_2U_2\}$	0.656(09)	0.699(14)	0.693(11)	0.676(08)			
$\{U_1U_2U_3\}$	0.642(10)	0.690(17)	0.685(12)	0.665(09)			
$\{U_1U_3U_3\}$	0.629(09)	0.682(21)	0.678(13)	0.654(09)			
$\{U_2U_2U_2\}$	0.635(08)	0.686(18)	0.680(12)	0.659(08)	0.644(11)	0.683(12)	0.664(08)
$\{U_2U_2U_3\}$	0.622(10)	0.678(22)	0.673(14)	0.649(10)			
$\{U_2U_3U_3\}$	0.609(11)	0.670(27)	0.667(16)	0.639(11)			
$\{U_3U_3U_3\}$	0.596(13)	0.661(33)	0.662(18)	0.628(14)	0.612(13)	0.660(22)	0.636(13)

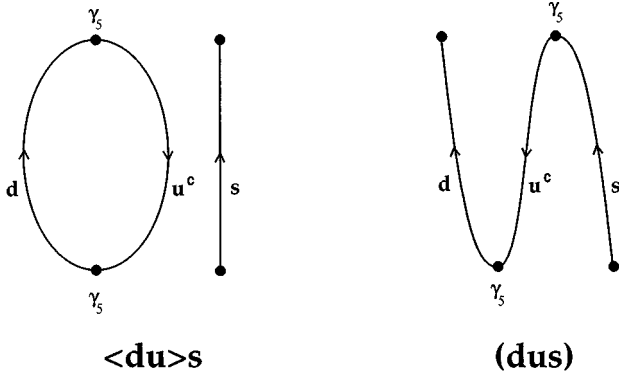


FIG. 8. Two different types of contractions for the baryon states.

sult. The higher order terms we use are motivated by quenched chiral perturbation theory which predicts nonanalytic terms of $O(m_q^{3/2})$ and analytic terms proportional to m_q^2 . The form of these terms and some predictions for their coefficients have been worked out in Ref. [24]. We attempt only a qualitative comparison with these predictions, though we provide the results of our fits so that others can pursue this further.

We first consider the octet hyperfine splitting “ $\Sigma - \Lambda$,”

$$\begin{aligned} \frac{M_{A\{BB\}} - M_{A[BB]}}{m_A - m_B} &= (-8D/3) + d_1 \frac{M_{AB}^3 - M_{BB}^3}{m_A - m_B} \\ &+ d'_1 \frac{M_{AA}^3 - M_{BB}^3}{m_A - m_B} + e_1 m_B \\ &+ e'_1(m_A + m_B), \end{aligned} \quad (7.14)$$

where M_{AB} is the mass of the pion with flavor $\bar{A}B$, etc. The constants d_i and e_i can be expressed in terms of parameters of the quenched chiral Lagrangian. For reasonable choices of these parameters, one expects $|d'_1| \ll |d_1|$. There is no useful information concerning e_1 or e'_1 .

We fit our results in two ways. First, we assume that the d_1 term is dominant and plot our data versus $(M_{AB}^3 - M_{BB}^3)/(m_A - m_B)$. The outcome is shown in Fig. 9. The data should collapse onto a single curve, which should be linear, and our results are reasonably consistent with this. What is particularly striking, however, is the size of the slope. This is a clear sign that terms of higher order than linear in the quark mass are needed to describe our baryon masses—recall that the linear term has been divided out in this fit. If we extrapolate linearly to the physical point ($m_A = m_s$, $m_B = \bar{m}$), we find [the fit gives $D = -0.36(3)$, $d_1 = -0.19(2) \text{ GeV}^{-2}$]

$$M_\Sigma - M_\Lambda = 76(7) \text{ MeV}. \quad (7.15)$$

It is conventional to quote this result in terms of an effective D parameter,

$$D_{\text{eff}} \equiv \frac{3(M_\Sigma - M_\Lambda)}{8(m_s - \bar{m})} = \frac{-29(3) \text{ MeV}}{m_s - \bar{m}} = -0.28(3). \quad (7.16)$$

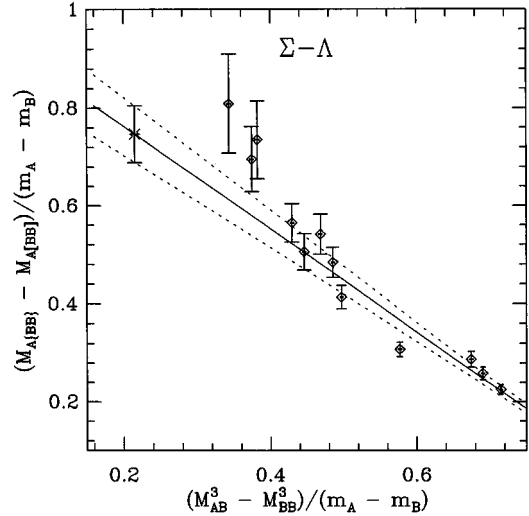


FIG. 9. Test for chiral corrections in $M_\Sigma - M_\Lambda$. The value extrapolated to the physical point is shown by the burst symbol at the extreme left. In this and subsequent figures, all masses are in lattice units.

Here (and in the similar estimates of D_{eff} and F_{eff} below), we use the nonperturbative definition of the $\overline{\text{MS}}$ quark mass calculated in MeV, but depart from our usual practice by evaluating it at the scale 2 GeV (instead of $1/a$). Note that D_{eff} differs from the D appearing in chiral expansions such as Eq. (7.14), for it absorbs some of the higher order terms.

In our second fit we test to see whether our data can be represented as well by the analytic terms. We have found, by trial and error, that Eq. (7.14) with $d_1 = d'_1 = 0$ and $e_1 = e'_1$ does a reasonable job; the plot is shown in Fig. 10. In this plot we have included the results for baryons composed of completely nondegenerate quarks, based on the discussion following Eqs. (7.11) and (7.12). To emphasize this, we have labeled the x axis by $m_u + m_d + m_s$ instead of $m_A + 2m_B$. The data show definite curvature, and so we have extrapolated to

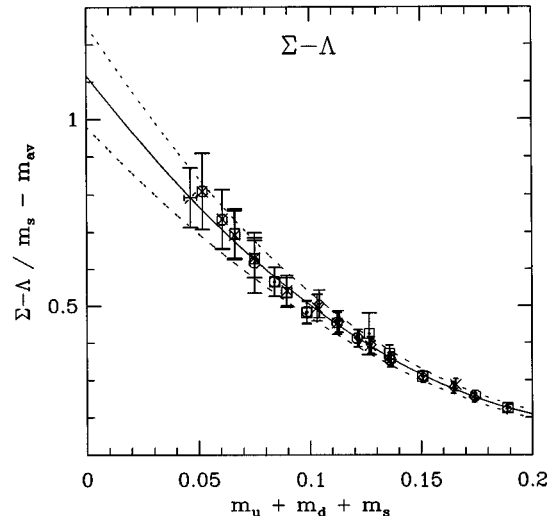


FIG. 10. Quadratic fit to $M_\Sigma - M_\Lambda/(\bar{m} - m_s)$, including baryons composed of completely nondegenerate quarks. The value extrapolated to the physical point is shown by the burst symbol at the extreme left.

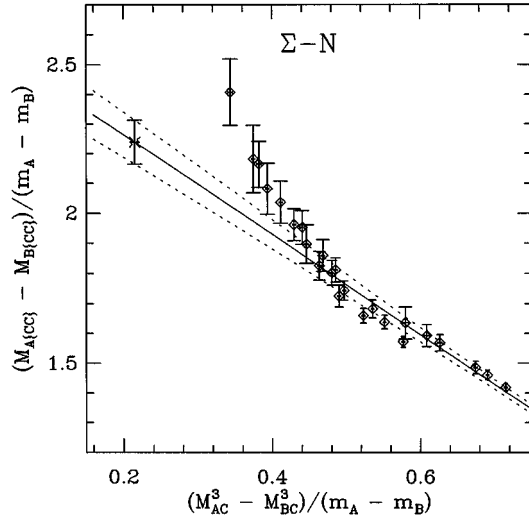


FIG. 11. Test for chiral corrections in $M_\Sigma - M_N$ as described in Eq. (7.18). The physical point is shown by the burst symbol at the extreme left.

the physical point using a quadratic fit (corresponding to terms up to m_q^3 in the original expression for baryon masses). The fit yields

$$M_\Sigma - M_\Lambda = 80(8) \text{ MeV}, \quad (7.17)$$

$$D_{\text{eff}} = \frac{-30(3) \text{ MeV}}{(m_s - \bar{m})} = -0.29(3).$$

These results are consistent with those from the “ $m_q^{3/2}$ ” fit.

Next we consider the “ Σ - N ” splitting, i.e., that between two Σ -like states having different strange quark masses. The chiral expansion is

$$\begin{aligned} \frac{M_{A\{CC\}} - M_{B\{CC\}}}{m_A - m_B} &= 2(F - D) + d_2 \frac{M_{AC}^3 - M_{BC}^3}{m_A - m_B} \\ &+ d'_2 \frac{M_{AA}^3 - M_{BB}^3}{m_A - m_B} + e_2 m_C \\ &+ e'_2(m_A + m_B). \end{aligned} \quad (7.18)$$

Chiral perturbation theory suggests that $|d'_2| < |d_2|$. Thus we first plot the data assuming d_2 is the dominant coefficient (Fig. 11). The collapse onto a single curve is reasonable, and a linear fit [$F - D = 1.30(5)$, $d_2 = -0.31(3) \text{ GeV}^{-2}$] gives

$$M_\Sigma - M_N = 227(14) \text{ MeV},$$

$$F_{\text{eff}} - D_{\text{eff}} = \frac{114(7) \text{ MeV}}{(m_s - \bar{m})} = 1.11(7). \quad (7.19)$$

We also have investigated various analytic fits, none of which do a good job of collapsing the data onto a single curve. Our best attempt, shown in Fig. 12, assumes $d_2 = d'_2 = 0$ and $e_2 = e'_2/4$; i.e., we plot against the average mass of the quarks in the two baryons. We again include nondegenerate baryons in this plot. Since the collapse is not good, we use two different extrapolations to the physical point. The first is a quadratic fit in the average mass as shown in Fig.

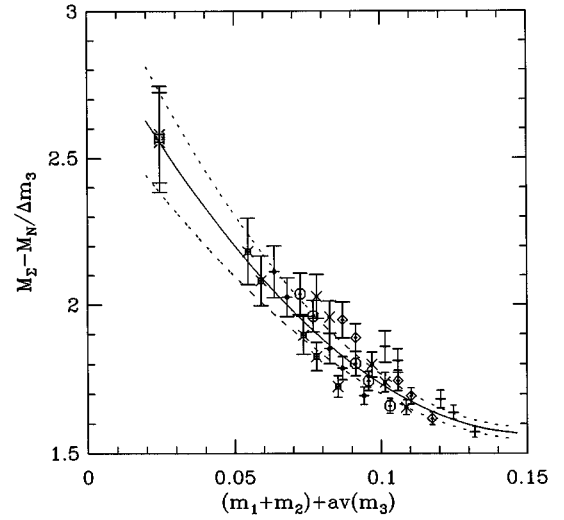


FIG. 12. Quadratic fit to $(M_\Sigma - M_N)/(m_s - \bar{m})$ for the 30 quark combinations. The results of the two ways of extrapolating to the physical value described in the text are shown by the burst symbols.

12. In the second we first extrapolate linearly to $m_B = m_C = \bar{m}$ and then interpolate to $m_A = m_s$. These two methods give almost identical results, as shown by the two “bursts” in the plot. The mean of these two points gives

$$M_\Sigma - M_N = 260(20) \text{ MeV},$$

$$F_{\text{eff}} - D_{\text{eff}} = \frac{130(10) \text{ MeV}}{(m_s - \bar{m})} = 1.27(10). \quad (7.20)$$

The difference between the two estimates, Eqs. (7.19) and (7.20), is indicative of the fact that neither of the forms fits all the data well.

Third, we consider the difference “ Ξ - N ,” in which we study the effect of changing the mass of the two symmetrized quarks. We expect

$$\begin{aligned} \frac{M_{A\{BB\}} - M_{A\{CC\}}}{m_B - m_C} &= 4F + d_3 \frac{M_{AB}^3 - M_{AC}^3}{m_B - m_C} + d'_3 \frac{M_{BB}^3 - M_{CC}^3}{m_B - m_C} \\ &+ e_3 m_A + e'_3(m_B + m_C). \end{aligned} \quad (7.21)$$

It turns out that in quenched chiral perturbation theory we expect $d_3 = d_2$ and $e_3 = e_2$. In this case, there is no expectation that d_3 and d'_3 should be substantially different in magnitude. Nevertheless, for simplicity, we first plot the data assuming d_3 is the dominant coefficient, as shown in Fig. 13. The data collapse reasonably onto a single curve, and a linear fit [$F = 0.92(3)$, $d_3 = -0.30(3) \text{ GeV}^{-2}$] yields

$$M_\Xi - M_N = 338(19) \text{ MeV}, \quad F_{\text{eff}} = \frac{84(5) \text{ MeV}}{(m_s - \bar{m})} = 0.82(5). \quad (7.22)$$

A quadratic fit to the average quark mass (i.e., assuming $e_3 = e'_3$) is slightly better, as shown in Fig. 14. The results are nevertheless consistent with those from the first fit:

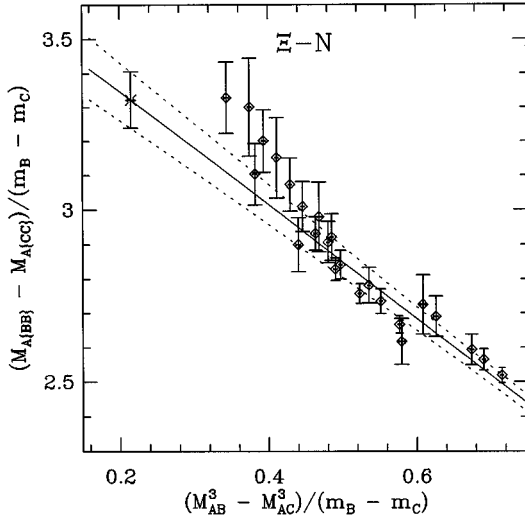


FIG. 13. Test for chiral corrections in $M_{\Xi} - M_N$ as described in Eq. (7.21). The physical point is shown by the burst symbol at the extreme left.

$$M_{\Xi} - M_N = 355(21) \text{ MeV}, \quad F_{\text{eff}} = \frac{89(5) \text{ MeV}}{(m_s - \bar{m})} = 0.87(5). \quad (7.23)$$

It is important to note that, once again, higher order corrections in the chiral expansion are substantial.

To further investigate the mass splittings we have considered the combination of differences appearing in the Gell-Mann–Okubo (GMO) formula $3M_{\Lambda} + M_{\Sigma} - 2M_N - 2M_{\Xi} = 0$. In our notation, this combination is

$$\text{GMO}(A, B) = 3M_{A[BB]} + M_{A\{BB\}} - 2M_{B\{BB\}} - 2M_{B\{AA\}}. \quad (7.24)$$

It is constructed to cancel the $O(m_q)$ terms,

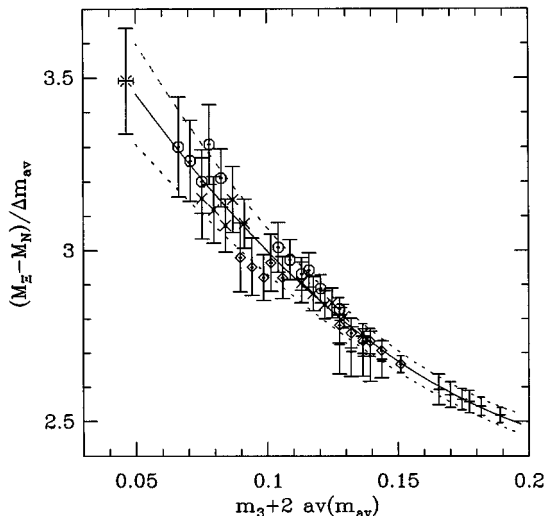


FIG. 14. Quadratic fit to $(M_{\Xi} - M_N) / (m_{\text{av}}^{\Xi} - m_{\text{av}}^N)$ for 44 quark combinations. The result of the quadratic extrapolation to the physical value is shown by the burst symbol.

TABLE XII. Tests of the Gell-Mann–Okubo mass formula: results for GMO (A, B) .

A	B	Method 1	Method 2	Method 3
S	U_1	0.000(01)	0.002(01)	0.001(01)
S	U_2	0.003(03)	0.003(03)	0.003(02)
S	U_3	0.008(08)	0.002(09)	0.005(04)
U_1	S	0.002(02)		
U_1	U_2	0.001(01)	0.000(02)	0.000(01)
U_1	U_3	0.003(05)	0.000(06)	0.002(02)
U_2	S	0.005(02)		
U_2	U_1	0.001(01)	0.001(01)	
U_2	U_3	-.001(04)		
U_3	S	0.009(05)		
U_3	U_1	0.005(04)	0.003(02)	
U_3	U_2	0.003(04)		

$$\text{GMO}(A, B) = d_4(M_{AA}^3 - 2M_{AB}^3 + M_{BB}^3) + e_4(m_A - m_B)^2 + \dots, \quad (7.25)$$

making it an interesting window on higher order terms. We have calculated $\text{GMO}(A, B)$ using three methods: (1) simply taking the differences of the masses; (2) using

$$\text{GMO}(A, B) = 4[M_{A\{BB\}} - M_{B\{BB\}}] - 3[M_{A\{BB\}} - M_{A[BB]}] - 2[M_{B\{AA\}} - M_{B\{BB\}}], \quad (7.26)$$

where the differences within square brackets are calculated from ratios of correlators; and (3) using another combination of differences (calculated using ratios),

$$\text{GMO}(A, B) = [M_{A\{BB\}} - M_{B\{BB\}}] + 3[M_{A[BB]} - M_{B\{BB\}}] - 2[M_{B\{AA\}} - M_{B\{BB\}}]. \quad (7.27)$$

Our results are given in Table XII. They are consistent with zero for all quark mass combinations, showing that higher order chiral corrections are not uniformly large. This is in qualitative agreement with experiment, where the GMO relation works well: $\text{GMO} = 26 \text{ MeV}$ or $\text{GMO} = 0.011$ in lattice units. It is difficult to make a quantitative comparison since we cannot extrapolate our data to the physical point. We note, however, that our results for the largest mass splitting, $A/B = S/U_3$, are consistent with the experimental value.

A summary of mass splittings in the octet multiplet is given in Table XIII. Several comments are in order. First, the “ $m_q^{3/2}$ ” fits show evidence for curvature, which, if included, would likely make the results agree more closely with those

TABLE XIII. Estimates of mass splittings in the baryon octet, using various fits explained in the text. Experimental results are given for comparison. All results are in MeV.

Fit	$m_q^{3/2}$	m_q^2	Eq. (7.9)	Expt.
$M_{\Sigma} - M_N$	227(13*)	260(20*)	194(12*)	253
$M_{\Xi} - M_N$	338(19*)	355(21*)	306(22*)	375
$M_{\Xi} - M_{\Sigma}$	107 (9*)	109 (8*)	112(14*)	122
$M_{\Sigma} - M_{\Lambda}$	76 (7*)	80 (8*)		77

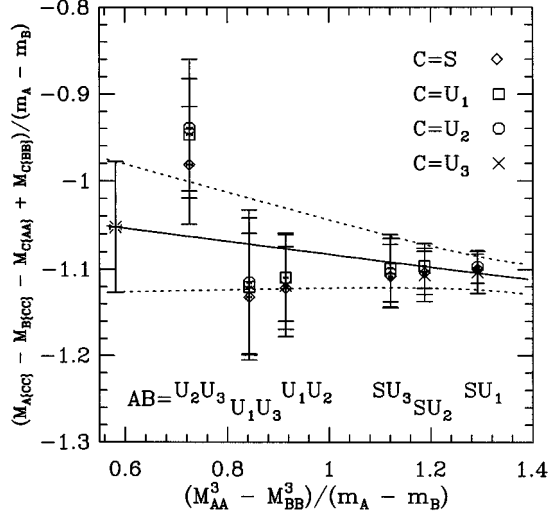


FIG. 15. The quantity X_Σ determined from fits to the ratio of correlators. The extrapolated value from which $M_\Xi - M_\Sigma$ is calculated is given by the burst symbol at the left.

from the “ m_q^2 ” fits. Second, we reiterate that the data are extremely poorly represented by the first order mass formulas Eq. (7.9)—this would predict that all the curves in Figs. 9–14 are flat. If, nevertheless, we fit to the linear terms, we find the results listed in the third column. Finally, we note the good agreement of the results from the m_q^2 fit (which are our most reliable) with the experimental splittings.

To further investigate the applicability of quenched chiral perturbation theory, we have constructed several other quantities. Although most of these are peculiar to the quenched approximation, having no counterpart in QCD, they allow us to see how well we understand the extrapolations that are needed for all quantities, including those which are physically relevant.

(1) We begin with the double difference

$$\begin{aligned} \frac{X_\Sigma(A,B,C)}{m_A - m_B} &= \frac{M_{A\{CC\}} - M_{B\{CC\}} - M_{C\{AA\}} + M_{C\{BB\}}}{m_A - m_B} \\ &= -2(F+D) + (d'_2 - d'_3) \frac{M_{AA}^3 - M_{BB}^3}{m_A - m_B} \\ &\quad + (e'_2 - e'_3)(m_A + m_B). \end{aligned} \quad (7.28)$$

This is interesting for several reasons. First, the expected chiral form is simpler than the differences considered above. Second, for $C=B$ or $C=A$, X_Σ reduces to $M(A\{BB\}) - M(B\{AA\})$, which for $A=s$ and $B=u$ is $m_\Xi - m_\Sigma$. Third, X_Σ is predicted to be independent of m_C . Strictly speaking, this is true up to quenched artifacts proportional to δ . Thus the m_C dependence of X_Σ is a window onto such artifacts. Our data for X_Σ , plotted in Fig. 15, confirm our expectations. There is no significant dependence on m_C —indeed, there is barely any dependence on m_A or m_B either. The fit yields $F+D=0.50(6)$ and $d'_2 - d'_3 = -0.013(16)$ GeV^{-2} assuming $e'_2 - e'_3 = 0$. Clearly, we could just as well fit with the e' terms. If we extrapolate to the physical point (assuming $M_{ss}^2 = 2M_K^2 - M_\pi^2$), we find

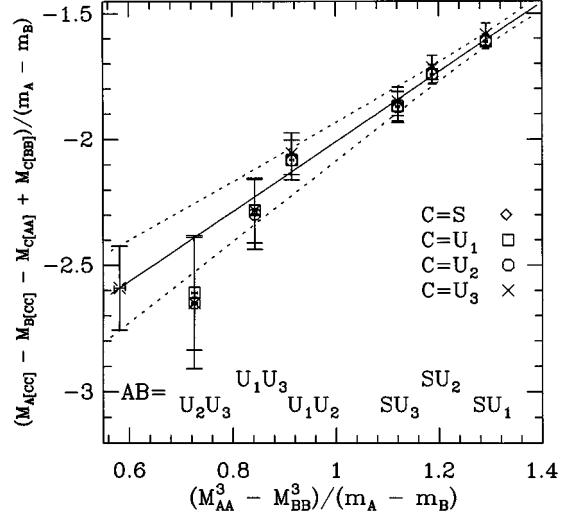


FIG. 16. The quantity X_Λ determined from the masses of the individual states. The point for physical quark masses is shown by the burst symbol at the left.

$$M_\Xi - M_\Sigma = 107(9) \text{ MeV},$$

$$(F_{\text{eff}} + D_{\text{eff}}) = \frac{53(5) \text{ MeV}}{(m_s - \bar{m})} = 0.52(5), \quad (7.29)$$

consistent with the other estimates given in Table XIII. It is noteworthy that the extrapolation required is minimal, unlike that for most of the mass differences considered above.

(2) We next consider the corresponding quantity for the Λ -like baryons,

$$\begin{aligned} \frac{X_\Lambda(A,B,C)}{m_A - m_B} &= \frac{M_{A\{CC\}} - M_{B\{CC\}} - M_{C\{AA\}} + M_{C\{BB\}}}{m_A - m_B} \\ &= -2F + 10D/3 + d_5 \frac{M_{AA}^3 - M_{BB}^3}{m_A - m_B} \\ &\quad + e_5(m_A + m_B). \end{aligned} \quad (7.30)$$

This always involves a quenched particle with no correspondent in nature, e.g., $M(U[SS])$. We plot X_Λ in Fig. 16. Again, the expectation of no dependence on m_C is borne out, but this time there are significant higher order terms. The fit yields $2F - 10D/3 = 3.4(3)$ and $d_5 = 0.26(4)$ GeV^{-2} , assuming $e_5 = 0$. The data are equally well described using an e_5 term with $d_5 = 0$.

(3) In the quenched approximation, we can form two additional double differences, analogous to $\text{GMO}(A,B)$, in which the $O(m_q)$ terms cancel:

$$Y_\Sigma(A,B,C,D) = M_{A\{CC\}} - M_{B\{CC\}} - M_{A\{DD\}} + M_{B\{DD\}}, \quad (7.31)$$

$$Y_\Lambda(A,B,C,D) = M_{A\{CC\}} - M_{B\{CC\}} - M_{A\{DD\}} + M_{B\{DD\}}.$$

Y_Σ picks out the d'_2 and e'_2 terms in Eqs. (7.18) and (7.28). The predicted form is

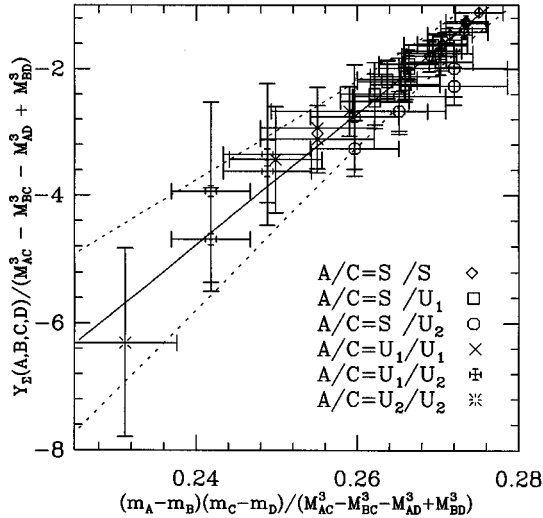


FIG. 17. Testing the mass dependence of Y_Σ (itself determined from fits to the ratio of correlators).

$$\begin{aligned} & \frac{Y_\Sigma(A,B,C,D)}{M_{AC}^3 - M_{BC}^3 - M_{AD}^3 + M_{BD}^3} \\ &= d_2 + e_2 \frac{(m_A - m_B)(m_C - m_D)}{M_{AC}^3 - M_{BC}^3 - M_{AD}^3 + M_{BD}^3}. \end{aligned} \quad (7.32)$$

We test this in Fig. 17. What is most noteworthy is that, unlike the GMO relation, there are significant higher order corrections. We find a reasonable fit if $d_2 \approx -5.4(1.4) \text{ GeV}^{-2}$ and $e_2 \approx 44(11) \text{ GeV}^{-1}$. The large errors in the fit parameters are due to the fact that the two variables $M_{AC}^3 - M_{BC}^3 - M_{AD}^3 + M_{BD}^3$ and $(m_A - m_B)(m_C - m_D)$ are nearly proportional for our set of quark masses. There is thus a significant cancellation between the two terms in the fit. Indeed, we can obtain as good a fit setting $e_2 = 0$ and replacing it with a higher order term proportional to $m_A + m_B + m_C + m_D$.

(4) Finally, we consider Y_Λ , which is expected to have the same functional form as Y_Σ . The data, shown in Fig. 18,

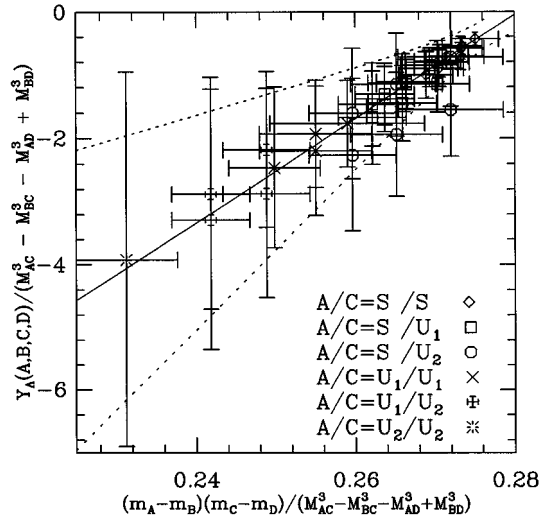


FIG. 18. Quantity Y_Λ determined from the masses of the individual states.

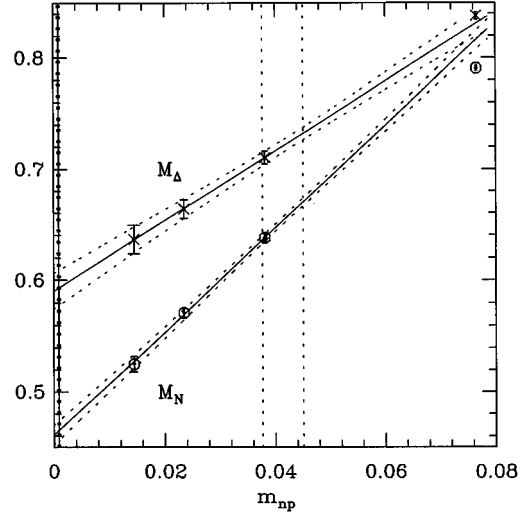


FIG. 19. Linear fit to M_N and M_Δ for the three $U_i U_j U_k$ quark combinations. The fourth degenerate point SSS is also shown.

are again consistent with the expected form, although the errors are larger since Y_Λ is calculated from masses instead of mass differences. The fit gives $-4.3(2.4) \text{ GeV}^{-2}$ for the intercept and $35(20) \text{ GeV}^{-1}$ for the slope.

In summary, we have demonstrated that terms beyond linear order in the quark mass are necessary to fit the octet baryon mass splittings. The lever arm provided by our four “light” quark masses is not, however, strong enough to disentangle the $m^{3/2}$ and m^2 contributions. Indeed, it is important to note that, if we did not have results for the baryons containing the S quark, our evidence for higher order terms would have been much weaker and our data would have been reasonably well fit by an $O(m)$ term alone. This would, however, have led to underestimates of all the mass differences, particularly $m_\Sigma - m_N$.

C. Nucleon mass

We now turn to the overall mass scale of the spin-1/2 baryons, which we set using the nucleon mass. As for the mass splittings, we expect to need terms of higher order than linear in the chiral expansion to describe our data, and so we analyze the data with and without them. We first fit to the masses of the baryons containing three degenerate quarks. The data are shown in Fig. 19 (along with those for the spin-3/2 baryons). We begin with a linear fit to the lightest three baryons, yielding the fit shown in the figure. We find

$$M_N = 0.461(9) + 4.7(2)\bar{m} = 1084(27) \text{ MeV}.$$

Next, we fit all four masses including an $m_q^{3/2}$ term, yielding $M_N = 1070(35) \text{ MeV}$. Finally, we fit all four masses including an m_q^2 term, which gives $M_N = 1072(31) \text{ MeV}$. In the last two cases we have included the same form for the higher order corrections in M_ρ for the determination of the scale and \bar{m} . Thus the inclusion of curvature systematically reduces M_N/M_ρ by about 0.5σ , although the precise functional form of the higher order terms is not resolved. For our best estimate we take the mean of the last two estimates, i.e., $M_N = 1071(35) \text{ MeV}$, corresponding to $a^{-1}(M_N) = 2062(56) \text{ MeV}$.

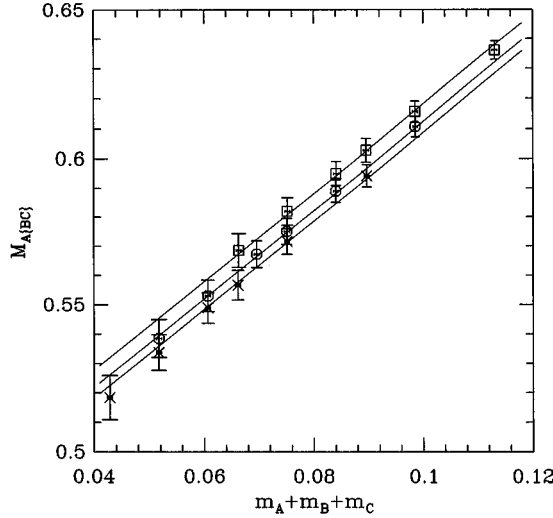


FIG. 20. Global fit to nucleon data using Eq. (7.9). The six cases for $m_A = U_1$ are shown by square symbols, $m_A = U_2$ by octagons, and $m_A = U_3$ by crosses.

The analysis of the previous paragraph is based on our full sample of lattices. Most of our results for mass differences came, by contrast, from our subsample of 110 lattices. Thus it is interesting to repeat the extraction of m_N on this subsample. We find that the results are slightly lower, though consistent within errors. For example, the linear “three point fit” to the lightest degenerate baryons yields $M_N = 0.446(9) + 5.04(21)\bar{m} = 1051(26)$ MeV, about 1σ below the corresponding result from the full sample. Using the subsample, however, we can attempt a global fit including baryons with nondegenerate quarks. We have done this using the Σ -like baryons composed of U_i quarks, fitting them to the linear chiral form of Eq. (7.9). We include all eighteen $U_A\{U_B U_C\}$ correlators, using the prescription of Eq. (7.13). The fit, shown in Fig. 20, gives

$$\begin{aligned} M_N &= 0.452(9^*) + 1.91(8^*)m_A + 3.01(16^*)(m_B + m_C)/2 \\ &= 1064(26^*) \text{ MeV.} \end{aligned}$$

This is in excellent agreement with the three point fit. The fact that the fit is reasonable underscores the point made above that the need for higher order terms is not apparent using the U_i quarks alone. A similar statement holds for the Λ -like states.

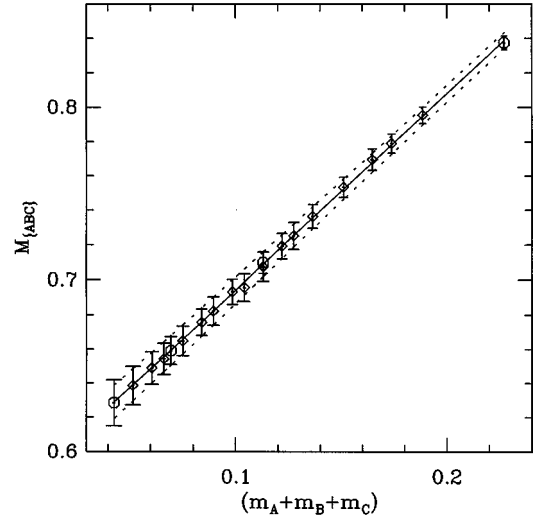


FIG. 21. Linear fit to M_{decuplet} for the 20 quark combinations. The four degenerate cases are shown with an octagon symbol.

D. Spin-3/2 baryon mass splittings

The analysis of the masses of the spin-3/2 baryons is more straightforward. As noted above, the correlators are labeled $\{ABC\}$ and are completely symmetric between the three flavors. We can form 20 states with our four masses, and none of these mix with each other.

As for the spin-1/2 baryons, we first concentrate on mass splittings. The chiral expansion for the spin-3/2 masses has been worked out for the case of three non degenerate quarks [24] and is (excluding quenched artifacts proportional to δ)

$$\begin{aligned} M_{\{ABC\}} &= M_0 + \Delta M + c^\Delta(m_A + m_B + m_C) + d_1^\Delta(M_{AB}^3 + M_{BC}^3 \\ &\quad + M_{CA}^3) + d_2^\Delta(M_{AA}^3 + M_{BB}^3 + M_{CC}^3) + e_1^\Delta(m_A m_B \\ &\quad + m_B m_C + m_C m_A) + e_2^\Delta(m_A^2 + m_B^2 + m_C^2). \end{aligned} \quad (7.33)$$

ΔM is the decuplet-octet splitting in the chiral limit. In contrast to the spin-1/2 baryons the terms of higher order than linear in the quark mass are small. This is shown in Fig. 21, in which we give the result of a linear fit to all 20 masses. We have also done linear fits to the 10 baryons composed of U_i quarks, and to the 3 lightest baryons composed of degenerate quarks. We refer to these three fits as “20-point,” “10-point,” and “3-point” fits, respectively. The results are consistent with one another:

$$M_{\text{decuplet}} = 0.590(16) + 3.18(34)m_q, \quad \text{3-point fit (full sample),}$$

$$M_{\text{decuplet}} = 0.578(16^*) + 3.49(33^*)m_q, \quad \text{3-point fit,}$$

$$M_{\text{decuplet}} = 0.578(16^*) + 3.50(34^*)(m_A + m_B + m_C)/3, \quad \text{10-point fit,}$$

$$M_{\text{decuplet}} = 0.580(12^*) + 3.42(14^*)(m_A + m_B + m_C)/3, \quad \text{20-point fit,} \quad (7.34)$$

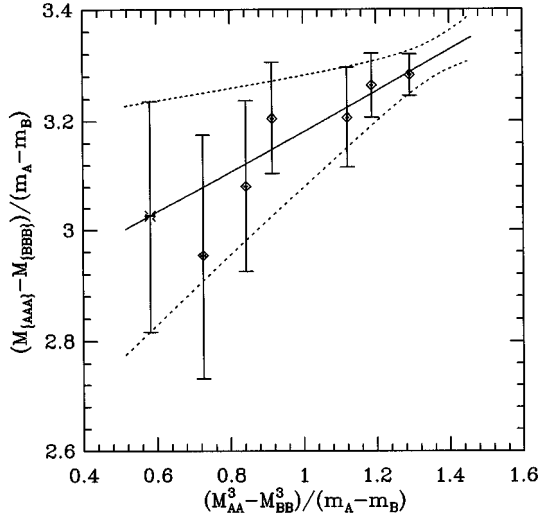


FIG. 22. $M_\Omega - M_\Delta$ mass splitting. The physical point is shown by the burst symbol at the left.

although there is a small systematic difference between the results from the full sample and the subsample.

The higher order terms, though small, are nevertheless present. We have investigated them using fits to ratios of correlators. We first consider $M_\Omega - M_\Delta$, which is obtained by fitting our data to

$$\frac{M_{\{AAA\}} - M_{\{BBB\}}}{m_A - m_B} = 3c^\Delta + 3(d_1^\Delta + d_2^\Delta) \frac{M_{AA}^3 - M_{BB}^3}{m_A - m_B} + 3(e_1^\Delta + e_2^\Delta)(m_A + m_B). \quad (7.35)$$

As before, we can fit our data keeping either the $d_1^\Delta + d_2^\Delta$ or the $e_1^\Delta + e_2^\Delta$ term. The former fit is shown in Fig. 22 and has parameters $c^\Delta = 0.94(12)$ and $d_1^\Delta + d_2^\Delta = 0.023(16) \text{ GeV}^{-2}$. The slope is small and marginally significant. Extrapolating to the physical point (using $M_{ss}^2 = 2M_K^2 - M_\pi^2$) yields $M_\Omega - M_\Delta = 308(24) \text{ MeV}$.

We have also done the extrapolation using a more traditional method: We calculate $M(\{AAA\}) - M(\{BBB\})$ for $B = U_i$ and $A = S$ or U_1 , extrapolate linearly to $m_B = \bar{m}$, and then interpolate linearly to $m_A = m_s$. We refer to this as the ‘‘3-point ratio’’ method. The result is $M_\Omega - M_\Delta = 316(18) \text{ MeV}$ and is consistent with our $m_q^{3/2}$ estimate. The result from our subsample, $310(19^*) \text{ MeV}$, is consistent.

We have repeated this analysis for the other two physically interesting mass splittings and collect the results in Table XIV. We only quote results from the ‘‘3-point ratio’’ extrapolations, since, with such mild deviations from linear-

TABLE XIV. Estimates of mass splittings in the baryon decuplet. The different methods are explained in the text. All results are in MeV.

State	Ratio 3 point	Eq. (7.34)	
		20 point	Expt.
$M_{\Sigma^*} - M_\Delta$	107(6*)	116(7*)	151
$M_{\Xi^*} - M_\Delta$	215(12*)	232(14*)	299
$M_\Omega - M_\Delta$	316(18)	347(21*)	436

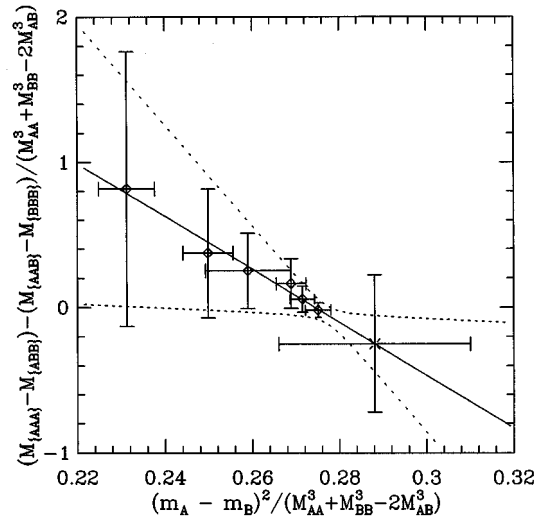


FIG. 23. Test of violations of the equal-spacing rule, Eq. (7.38). The physical point is indicated by the burst symbol, here at the right.

ity, any reasonable extrapolation method using our ratio data gives almost the same result. We also include the results of extrapolating using the parameters from the 20-point linear fit. The small difference between the two sets of results is due to the higher order terms. Both sets of results are significantly smaller than the experimental splittings, and the inclusion of the higher order terms makes the disagreement worse. These features are in marked contrast to those we saw in the spin-1/2 baryons.

We can study the higher order terms in more detail by looking at violations of the ‘‘equal-spacing rule’’

$$M_{\{AAA\}} - M_{\{AAB\}} = M_{\{AAB\}} - M_{\{ABB\}} = M_{\{ABB\}} - M_{\{BBB\}}. \quad (7.36)$$

This rule holds when keeping up to the linear term in the chiral expansion. Experimentally, the three splittings are $M_\Omega - M_{\Xi^*} = 137.5 \text{ MeV}$, $M_{\Xi^*} - M_{\Sigma^*} = 148.1 \text{ MeV}$, and $M_{\Sigma^*} - M_\Delta = 151 \text{ MeV}$. The violations of the rule are thus small, and it is interesting to see how well the quenched approximation reproduces the magnitude and pattern of these violations. We consider two double differences

$$\text{ES1}(A, B) = (M_{\{AAA\}} - M_{\{AAB\}}) - (M_{\{ABB\}} - M_{\{BBB\}}), \quad (7.37)$$

$$\text{ES2}(A, B) = (M_{\{AAA\}} - M_{\{BBB\}}) - 3(M_{\{AAB\}} - M_{\{ABB\}}).$$

The first becomes $(M_\Omega - M_{\Xi^*}) - (M_{\Sigma^*} - M_\Delta) = -13 \text{ MeV}$ when $m_A = m_s$ and $m_B = \bar{m}$. The expectation from quenched chiral perturbation theory is that

$$\text{ES1}(A, B) = 2d_1^\Delta(M_{AA}^3 + M_{BB}^3 - 2M_{AB}^3) + 2e_1^\Delta(m_A - m_B)^2; \quad (7.38)$$

i.e., the form of the higher order terms is the same as that appearing in the GMO relation [Eq. (7.25)]. They are shown in Fig. 23 and are consistent with the expected chiral form [$d_1^\Delta = 0.46(43) \text{ GeV}^{-2}$, $e_1^\Delta = -8(7) \text{ GeV}^{-1}$], with large errors. Extrapolating to the physical point, we find $\text{ES1} = -4(7) \text{ MeV}$, marginally inconsistent with the experimental value.

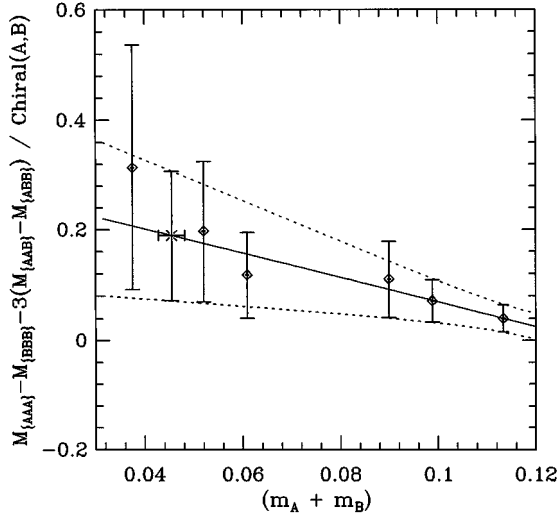


FIG. 24. Test of violations of the equal-spacing rule, Eq. (7.39). The physical point is indicated by the burst symbol (second from left).

The second double difference ES2 (A, B) is predicted to vanish by the general form of Eq. (7.33). The same is true in chiral perturbation theory in full QCD [25]. Thus it is a window onto the quenched artifacts proportional to δ , whose form is predicted to be [24]

$$\begin{aligned} \text{ES2}(A, B) &= \delta f^\Delta \text{chiral}(A, B), \\ \text{chiral}(A, B) &= (m_A - m_B) \left(\ln(M_{AA}^2/M_{BB}^2) + 2 \right. \\ &\quad \left. - \frac{2M_{AA}^2 \ln(M_{AA}^2/M_{BB}^2)}{M_{AA}^2 - M_{BB}^2} \right). \end{aligned} \quad (7.39)$$

As explained in Sec. IV, we have omitted such artifacts from previous expressions, but we include them here so as to have a form to fit with. Note that the function $\text{chiral}(A, B)$ is antisymmetric under $A \leftrightarrow B$, as it must be in order to match the antisymmetry of the left-hand side. Note also that it diverges logarithmically when $m_A \rightarrow 0$, an example of the sickness of the quenched approximation in the chiral limit.

Our results, shown in Fig. 24, are statistically different from zero. We show a linear fit of $\text{ES2}(A, B)/\text{chiral}(A, B)$ versus $m_A + m_B$, which yields an intercept of $\delta f^\Delta = 0.29(19)$ and a slope of $-0.9(0.7) \text{ GeV}^{-1}$. Interpolating to the physical point, we find $\text{ES2} = -29(18) \text{ MeV}$. This has the same sign as the experimental value

$$M_\Omega - M_\Delta - 3(M_{\Xi^*} - M_{\Sigma^*}) = -8 \text{ MeV},$$

but its magnitude is much larger. It is important to realize, however, that our values for ES2 range from -1 to -10 MeV . The large value after extrapolation is due to the divergence of $\text{chiral}(A, B)$ as $m \rightarrow 0$. We have attempted analytic extrapolations, using a linear combination of $(m_A - m_B)^3$ and $(m_A - m_B)(m_A + m_B)^2$, but this ansatz does not fit our data.

The most important conclusion to be drawn from this analysis is that the decuplet splittings are smaller than the experimental values. This discrepancy is only made worse if

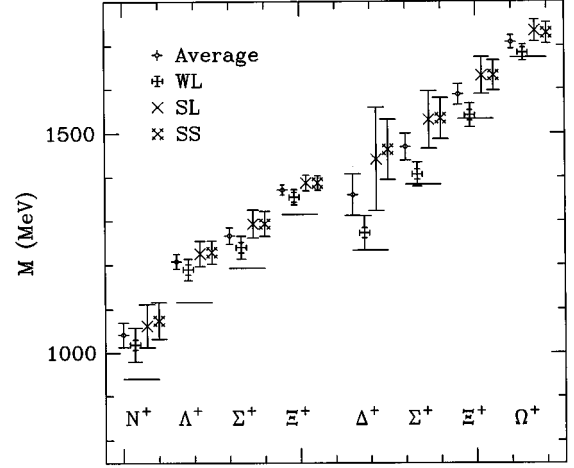


FIG. 25. Comparison of the baryon masses obtained in this calculation with the experimental data indicated by the horizontal lines. The scale a is set by M_ρ and the data for all states are from the sub sample of 110 lattices.

we use other definitions of the strange quark mass, e.g., $m_s(M_K)$. We have also found some evidence for artifacts due to quenching in the baryon spectrum. Given the size of our errors, however, this result is far from definitive.

E. M_Δ and $M_\Delta - M_N$

We close this section with our results for the overall scale of the spin-3/2 baryons and its relation to that of the spin-1/2 baryons. Our preferred value for M_Δ comes from the 3-point linear fit to the full sample (shown in Fig. 19), yielding $M_\Delta = 1382(36) \text{ MeV}$. Fits to the subsample, the parameters of which are given in Eq. (7.34), yield values that are consistent with one another, but lie slightly below that for the full sample. For example, the 20-point fit gives $M_\Delta = 1362(36^*) \text{ MeV}$. We have also tried 4-point fits to the degenerate states, including $m^{3/2}$ (or m^2) corrections in both Δ and ρ . These increase the estimates of M_Δ to 1410(48) [1395(43)], the bulk of the increase coming from the change in scale due to the curvature in M_ρ .

We have calculated $M_\Delta - M_N$ from the ratios of correlators using the full data sample. Using linear extrapolation from the three light mass points, we find 318(30) MeV. Including an $m_q^{3/2}$ or m_q^2 term in both $M_\Delta - M_N$ and M_ρ fits, we get 365(44) and 347(39), respectively. These values are slightly higher than the experimental value 293 MeV. A summary of our baryon mass results (without extrapolation to $a=0$) is shown in Fig. 25 along with the experimental data.

We have also made fits to the negative parity baryon states. The signal in the correlators is much poorer, falling below the noise by $t=12$. For this reason we only present the summary shown in Fig. 26.

VIII. INFINITE VOLUME CONTINUUM RESULTS

There exist three other high statistics calculations of the spectrum with Wilson fermions at $\beta=6.0$ on lattices of size 24^3 [26,27,7]. Their results are given in Table XV along with our best estimates. The data indicate that there are no signifi-

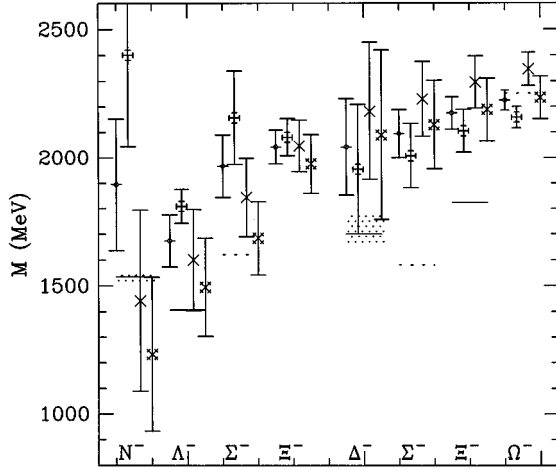


FIG. 26. Comparison of the negative parity baryon masses obtained in this calculation with the experimental data indicated by the horizontal lines. Shaded bands show the experimental uncertainty. The scale a is set by M_ρ and the data for all states are from the subsample of 110 lattices.

cant differences between the 24^3 and 32^3 lattices. Thus we do not apply any finite size corrections to our data.

Our best estimates at $\beta=6.0$ for various mass ratios of interest are

$$\begin{aligned} \frac{M_N}{M_\rho} &= 1.412(35), \quad \text{Expt. } 1.22, \\ \frac{M_\Delta}{M_\rho} &= 1.800(47), \quad \text{Expt. } 1.60, \\ \frac{M_\Delta}{M_N} &= 1.275(36), \quad \text{Expt. } 1.31. \end{aligned} \quad (8.1)$$

These are obtained by extrapolating individual masses linearly to \bar{m} and then taking ratios within the jackknife procedure. All extrapolations are done using only the U_i quarks. To check for extrapolation errors we have also calculated the ratios for each quark mass and then linearly extrapolated these to \bar{m} . This yields $M_N/M_\rho=1.42(3)$, $M_\Delta/M_\rho=1.79(4)$, and $M_\Delta/M_N=1.25(3)$, consistent with the first method.

TABLE XV. Comparison of hadron masses obtained using Wilson fermions at $\beta=6.0$. Results from $32^3 \times 64$ lattices are from the present work, while $24^3 \times 32$ data are from Ref. [26], $24^3 \times 54$ data are from Ref. [27], and $24^3 \times 64$ data are from Ref. [7].

κ	Size	Statistics	m_π	m_ρ	m_N	m_Δ
0.155	$24^3 \times 32$	78	0.298(2)	0.428(4)	0.647(6)	0.745(14)
0.155	$24^3 \times 54$	200	0.297(2)	0.422(4)	0.644(9)	0.728(11)
0.155	$32^3 \times 64$	170	0.296(1)	0.422(2)	0.638(3)	0.710(6)
0.155	$24^3 \times 64$	1000	0.2964(4)	0.423(2)	0.642(3)	
0.1558	$24^3 \times 32$	78	0.234(3)	0.397(5)	0.574(8)	0.686(25)
0.1558	$32^3 \times 64$	170	0.234(1)	0.387(3)	0.571(4)	0.664(8)
0.1563	$24^3 \times 32$	78	0.184(3)	0.378(10)	0.522(14)	0.636(45)
0.1563	$24^3 \times 54$	200	0.185(3)	0.353(15)	0.536(30)	0.670(53)
0.1563	$32^3 \times 64$	170	0.185(1)	0.361(5)	0.525(7)	0.636(13)

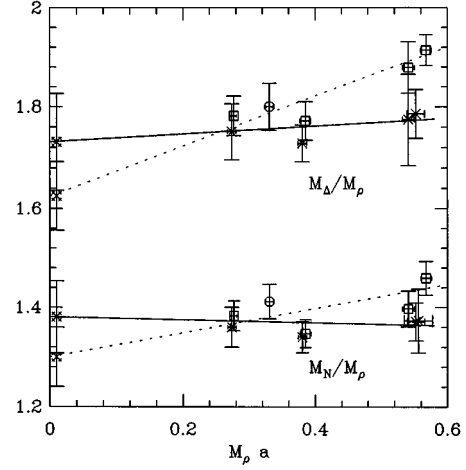


FIG. 27. Linear extrapolation to the continuum limit of the ratios M_N/M_ρ and M_Δ/M_ρ . Our data are shown as octagons, and the rest of the points are from the GF11 Collaboration [2]. The ‘‘012’’ sink points are labeled by squares and the sink ‘‘4’’ points by crosses. The extrapolated values are shown by fancy crosses and are shifted from $M_\rho a=0$ for clarity. At $\beta=5.7$ ($M_\rho a \approx 0.56$), we have shown the GF11 Collaboration’s data for both 16^3 and 24^3 lattices even though they used only the 16^3 data in the fit and shifted their continuum result by the difference to account for finite size effects.

Our results for M_N/M_ρ and M_Δ/M_ρ are larger than the experimental values. It has been stressed by the GF11 Collaboration, however, that these ratios have a significant dependence on a . In an attempt to check this we combine our results with those from the GF11 Collaboration [2] at $\beta=5.7$, 5.93, and 6.17. The two calculations have similar statistics, while the physical volume of our lattices is larger. The GF11 Collaboration have made two separate extrapolations to the continuum limit using different Gaussian smeared sinks. In their notation, ‘‘012’’ is a combination of results from three sinks with smearing radii 0, 1, and 2, while ‘‘4’’ refers to the use of a single larger smearing radius of size 4. In the final analysis they prefer to use the ‘‘012’’ result as it has smaller statistical errors. We update these two linear fits (using the same three data points used in [2] and ours at $\beta=6.0$), and the results are shown in Fig. 27. After including our point, the extrapolated values for the ‘‘012’’ data (dotted lines)

change from $M_N/M_\rho=1.28(7)$ to $1.30(6)$ and from $M_\Delta/M_\rho=1.61(8)$ to $1.62(7)$. The χ^2/N_{DF} for the new fits are 2.1 and 0.85, respectively. The analogous numbers for the sink “4” data (solid line) are $1.33(9)\rightarrow 1.38(7)$ and $1.68(10)\rightarrow 1.73(10)$ with χ^2/N_{DF} for the new fits equal to 1.2 and 0.86, respectively.

As is evident from Fig. 27, the main difference between the two fits comes from the difference in the “012” and “4” data at $\beta=5.7$. On the basis of χ^2/N_{DF} , we find that combining our results with the sink “4” GF11 data is preferred, in which case there is very little a dependence. If we neglect the point at strongest coupling $\beta=5.7$, then the remaining three points again show no clear a dependence for both M_N/M_ρ and M_Δ/M_ρ and give very similar values for the fit parameters.

The ambiguity in the extrapolation makes it clear that data at more values of β are needed in order to reliably extrapolate to the continuum limit. Our preferred estimates are $M_N/M_\rho=1.38(7)$ and $M_\Delta/M_\rho=1.73(10)$ from fits shown by a solid line in Fig. 27. This suggests that the quenched approximation is good to only $\sim 10\text{--}15\%$.

IX. CONCLUSIONS

We have presented a detailed analysis of the hadron spectrum in quenched QCD at $\beta=6.0$ with Wilson fermions, focusing on states composed of light quarks. Our small statistical errors and our use of several moderately light quarks have allowed us to improve the extrapolations to the chiral limit. This is particularly true of the mass splittings among the octet baryons. Here we find substantial contributions from terms of higher order than linear in the quark mass. Motivated by quenched chiral perturbation theory, we have found good variables with which to extrapolate to the physical quark masses. Our results show that the splittings are larger than previously thought and are comparable with their experimental values. These results emphasize the importance of calculating masses of baryons composed of several combinations of nondegenerate quarks.

The extrapolations required for the π , ρ , N , and Δ are less sensitive to higher order terms. There is a clear curvature in the ρ and nucleon channels, and it can be accommodated either by including a term of $O(m_q^{3/2})$ (which would result from chiral loops) or a term $O(m_q^2)$. The effect on the ex-

trapolated values for the M_ρ and M_N is, however, small, roughly comparable to the statistical errors. Higher order terms are also small for the decuplet baryons.

It is not surprising that higher order terms are needed when considering quarks with masses ranging up to and beyond that of the physical strange quark. In previous calculations of baryons composed of degenerate quarks, these terms were small and often neglected. What is striking is how this is not true for many of the mass differences involving baryons composed of nondegenerate quarks.

One caveat concerning the results for mass splittings is the fact that there are substantial systematic errors in the extraction of m_s . Different methods lead to results differing by up to $\sim 20\%$. This is presumably an error due to quenching, although some part of it could be due to discretization. Our favored choice for m_s is that determined by matching to the ratio M_ϕ/M_ρ . This gives the largest estimate for m_s .

How does the spectrum at $\beta=6$ compare with experiment? We find that the ratio $M_N/m_\rho=1.41(4)$ is too high, while $M_\Delta/M_N=1.27(4)$ is consistent with experiments. Using the larger estimate of m_s , the octet baryons splittings agree with experiment, while those in the decuplet are too small by 30%.

Of course it is quite possible that there is substantial variation in some of these ratios as we extrapolate to the continuum limit. Combining our data with that of the GF11 Collaboration, however, we conclude that there remains considerable uncertainty in this extrapolation. Our preferred extrapolation gives $M_N/M_\rho=1.38(7)$ and $M_\Delta/M_\rho=1.73(10)$, but the systematic errors exceed those from statistics. Thus, in our view, it remains an open question how well the quenched approximation represents full QCD when extrapolated to the continuum limit. The errors could well be as large as $\sim 10\text{--}15\%$.

ACKNOWLEDGMENTS

These calculations have been done on the CM5 computer at LANL as part of the U.S. DOE HPCC Grand Challenge program and at NCSA under a Metacenter allocation. We thank Jeff Mandula, Larry Smarr, Andy White, and the entire staff at the two centers for their tremendous support throughout this project.

-
- [1] T. Bhattacharya and R. Gupta, in “Lattice ’94,” proceedings of the International Symposium on Lattice Field Theory, Bielefeld, Germany, 1994, edited by F. Karsch *et al.* [Nucl. Phys. B (Proc. Suppl.) **42**, 935 (1995)].
- [2] GF11 Collaboration, Nucl. Phys. **B430**, 179 (1994).
- [3] R. Gupta *et al.*, Phys. Rev. D **44**, 3272 (1991).
- [4] R. Gupta *et al.*, Phys. Rev. D **40**, 2072 (1989).
- [5] A. Borici and P. deForcrand (private communication).
- [6] A. Frommer *et al.*, Int. J. Mod. Phys. C **5**, 1073 (1994).
- [7] JLQCD Collaboration, S. Aoki *et al.*, report, hep-lat/9510013 (unpublished).
- [8] C. Michael, Phys. Rev. D **49**, 2616 (1994); G. Kilcup, in “Lattice ’93,” proceedings of the International Symposium on Lattice Field Theory, Dallas, 1993, edited by T. Draper *et al.* [Nucl. Phys. B (Proc. Suppl.) **34**, 350 (1994)].
- [9] S. Sharpe, Phys. Rev. D **41**, 3233 (1990); **46**, 3146 (1992); 1994 TASI lectures, report, hep-ph/9412243 (unpublished).
- [10] C. Bernard and M. Golterman, Phys. Rev. D **46**, 853 (1992); M. Golterman, report, hep-lat/9405002 (unpublished).
- [11] R. Gupta, Nucl. Phys. B (Proc. Suppl.) **42**, 85 (1995).
- [12] M. Golterman, Acta Phys. Polon. **B25**, 1731 (1994).
- [13] S. Kim and D. K. Sinclair, Phys. Rev. D **52**, 2614 (1995).
- [14] J. Labrenz and S. Sharpe, “Lattice ’93” [8], p. 335.
- [15] E. Jenkins, A. Manohar, and M. Wise, Phys. Rev. Lett. **75**, 2272 (1995).

- [16] D. Daniel, R. Gupta, G. Kilcup, A. Patel, and S. Sharpe, Phys. Rev. D **46**, 3130 (1992).
- [17] P. Lepage and P. Mackenzie, Phys. Rev. D **48**, 2250 (1993).
- [18] C. Allton *et al.*, Nucl. Phys. **B431**, 667 (1994).
- [19] T. Bhattacharya and R. Gupta, Phys. Rev. D (to be published).
- [20] C. Davies *et al.*, Phys. Rev. D **50**, 6963 (1994).
- [21] J. Donoghue, B. Holstein, and D. Wyler, Phys. Rev. Lett. **69**, 3444 (1992).
- [22] P. Lacock and C. Michael, Phys. Rev. D **52**, 5213 (1995).
- [23] J. Sloan, "Lattice '94," [1], p. 171.
- [24] J. Labrenz and S. Sharpe (in preparation).
- [25] E. Jenkins, Nucl. Phys. **B368**, 190 (1992).
- [26] APE Collaboration, S. Cabasino *et al.*, Phys. Lett. B **258**, 195 (1991).
- [27] QCDPAX Collaboration, Y. Iwasaki *et al.*, in "Lattice '91," proceedings of the International Symposium on Lattice Field Theory, Tsukuba, Japan, 1991, edited by Fukugita *et al.* [Nucl. Phys. B (Proc. Suppl.) **26**, 281 (1992)]; and Report No. hep-lat/9512031 (unpublished).